Australia's National Science Agency

MD-WERP Report T2.7.6

Advancing Floodplain Inundation and Volume Prediction for Water Management

Jin Teng, Dave Penton, Catherine Ticehurst, Ang Yang, Steve Marvanek, Robert Bridgart, Jai Vaze, Fathaha Khanam, Cherry Mateo, Francis Chiew, Hongxing Zheng, Jenet Austin, David Post, Eilish Brennan

MD-WERP Project T2.RQ7

January 2025

Citation

Teng J, Penton D, Ticehurst C, Yang A, Marvanek S, Bridgart R, Vaze J, Khanam F, Mateo C, Chiew F, Zheng H, Austin J, Post D and Brennan E (2025) Advancing Floodplain Inundation and Volume Prediction for Water Management. CSIRO, Australia.

Foreword

This report presents a comprehensive summary of the research, datasets, and the floodplain inundation model developed for Research Question 7 (RQ7) – "Enhancing floodplain inundation and volume prediction to support environmental watering and water resource planning" a key component of the Murray-Darling Water and Research Program (MD-WERP). Over the three-year project duration, significant progress has been made in improving the prediction and understanding of floodplain inundation dynamics within the Murray-Darling Basin.

The report is structured into four main sections:

1. Review and Input Data Preparation: This section provides a review of existing literature, methodologies, and the extensive data preparation that underpins the model, datasets and relative research.
2. Research: Here, we delve into the core research activities, including the development of methods and approaches designed to enhance surface water detection from remote sensing imagery and a water depth estimation model that is essential for inundation volume predictions.
3. Datasets: This section outlines the datasets developed and utilized throughout the project, which serve as critical resources for modelling, validating floodplain responses, and investigating climate change impact on flooding.
4. RQ7 Model: Finally, the report details the RQ7 inundation model, a tool that synthesizes the research findings and data, aiming to offer more accurate predictions of floodplain water volume and spatial inundation patterns.

We hope that this report serves as a valuable resource for future research efforts in floodplain hydrology and contributes to more effective water management strategies within the Murray-Darling Basin.

Contents

Figures

Tables

Acknowledgments

This work was conducted at CSIRO Environment as part of the Murray–Darling Water and Environment Research Program (MD-WERP). The MD-WERP, an Australian Government initiative, aims to enhance scientific knowledge of the Murray–Darling Basin to support informed water and environmental management decisions. The program focuses on four priority research themes: Climate Adaptation, Hydrology, Environmental Outcomes, and Social, Economic, and Cultural Outcomes. Research Question 7 (RQ7) – *Enhancing Floodplain Inundation and Volume Prediction to Support Environmental Watering and Water Resources Planning* – is one of the projects within the Hydrology theme.

We extend our gratitude to Charlotte Dennis, Alistair Korn, Sohail Rai, and Georgia Koerber from the Murray–Darling Basin Authority (MDBA) for their continuous support in project management and assistance with data access. The project has been conducted in conjunction with the MDB Ecosystem Function Project and two CSIRO funded Digital Water and Landscape projects, fostering valuable collaboration across initiatives.

We also thank our collaborators for their contributions of data and expertise: Fazlul Karim, Carmel Pollino, Fareed Mirza (CSIRO); Leo Lymburner, Clair Krause (Geoscience Australia); Gareth Carpenter (SA Water); Amber Craig, Andrew Keogh, Jim Foreman, Stephen Sunderland, Ben Bradshaw, Gabrielle Hunt (MDBA); Nicholas Streeton, Ian Burns, Tim Morrison, Banu Hazrati, Michelle Cavallaro (NSW Department of Climate Change, Energy, the Environment and Water); Sam Davis, Anthony Townsend, David Cordina, Rodney Price, Matthew Miles and Joseph Brennan (NSW Department of Primary Industries); as well as Jonathan Marshall, Glenn McGregor, and Norbert Menke (Queensland Department of Environment, Science, and Innovation).

Finally, we pay our respects to the Traditional Owners and their Nations within the Murray–Darling Basin. We recognize and honour their enduring cultural, social, environmental, spiritual, and economic connection to their lands and waters.

Executive summary

The Research Question 7 (RQ7) project aims to build on the foundational models and capacities developed through previous research, advancing floodplain inundation modelling to support systematic management and scenario planning across the Murray–Darling Basin. This research, part of the Murray–Darling Water and Environment Research Program (MD-WERP), seeks to develop a model capable of performing multiple runs over large areas and extended simulation periods, providing robust predictions of flood inundation extent, depth, duration, and floodplain volume. The model is intended to support long-term, data-driven environmental and water resource planning, particularly under varying climate scenarios and management strategies.

Over the course of this project, we began with an extensive review and input data preparation phase, laying a robust foundation for the modelling work by examining existing literature and methodologies, and gathering comprehensive data on floodplain hydrology, topography, and climate. This initial phase enabled a detailed understanding of the critical elements needed for improved floodplain inundation modelling.

Our research activities focused on developing innovative methods to enhance the accuracy and coverage of floodplain inundation extent, depth, and volume predictions, tailored to the unique characteristics of the Murray–Darling Basin. Specifically, we developed advanced techniques for detecting surface water from remote sensing imagery and benchmarked water depth estimation models, critical for precise inundation volume calculations. These advancements support both dataset production and modelling development, forming a crucial basis for future applications.

We have created high-resolution datasets that include maps of inundation extents, water depth, persistent water presence, and the maximum number of consecutive dry years across the basin. These datasets are instrumental for quantifying flood characteristics and assessing the impacts of climate change on flooding patterns within the Murray–Darling Basin.

The core output of the project, the RQ7 Model, integrates these research findings and datasets into a predictive tool designed to provide reliable estimates of floodplain water volumes and spatial inundation patterns. The RQ7 Model offers a valuable resource for stakeholders such as the Murray–Darling Basin Authority (MDBA), Basin States, the Commonwealth Environmental Water Office (CEWO), and hydrological and environmental researchers. These users can leverage the model's capabilities to make informed decisions that balance ecological needs with resource availability under changing climate conditions, supporting resilient environmental water management and scenario planning across the basin.

In summary, the RQ7 project presents a significant advancement in floodplain modelling, with the RQ7 model providing a practical tool for current and future floodplain management across the basin. The knowledge, data, and tools developed in this project contribute to a more resilient approach to environmental water management and floodplain adaptation, helping safeguard the ecological and community well-being of the Murray–Darling Basin.

Part I Review and Input Data Preparation

1 Introduction

Flood inundation models are essential tools for supporting decision-making in environmental watering and water resource planning. Since the 1970s, systematic research efforts have significantly advanced model capabilities, resulting in various models with different complexities, data requirements, and computational demands, each suited to specific applications. Hydrodynamic models, in particular, are frequently employed to inform water resource management due to their detailed simulations. However, even with improvements in computational power, these models' high computational cost and data requirements limit their feasibility for large-scale, systematic management and scenario planning, which often requires extensive spatial coverage and multiple model runs.

The RQ7 research seeks to build on past modelling capacities to develop a model specifically designed for systematic management applications. This proposed model is a hybrid approach, combining aspects of the River Murray Floodplain Inundation Model (RiM-FIM) (Overton et al., 2006; Penton and Overton, 2007) and Teng-Vaze-Dutta (TVD)(Teng et al., 2018, 2015a) models: it creates a comprehensive database from remote sensing imagery, as RiM-FIM does, while incorporating a daily floodplain water extent and depth simulation based on hydrograph, similar to the TVD model. The RQ7 model aims to improve predictions of flood inundation extent, depth, duration, and floodplain volumes, making it a practical tool for large-scale planning and environmental management.

In the first year of the project, we reviewed widely used flood inundation models and key prior modelling efforts within the Murray–Darling Basin. We also collected, developed, and synthesized multiple datasets crucial for developing, constraining, and validating flood inundation models. These datasets include digital elevation models (DEMs), hydrodynamic model outputs, river stage heights, flow hydrographs and climate data. Throughout the project, we continuously refined these datasets, publishing them on the CSIRO data access portal whenever possible, except for those restricted by license agreements. These efforts have established a strong foundation for creating a reliable, large-scale flood inundation model tailored to the unique needs of the Murray–Darling Basin.

2 Commonly used flood inundation models

In the last century we have witnessed rapid advancement in the way we undertake flood inundation modelling. Two categories of approaches have attracted the most attention in the research community, with a third type gaining popularity in recent years. The two most commonly used approaches are empirical methods and hydrodynamic models, and the third type is conceptual models.

Table 1 compares the three approaches described above. They all have their own strengths and limitations and are suitable for different applications. In summary, the empirical method is most suitable for flood monitoring and post disaster assessment; the hydrodynamic models effectively simulate impact of dam break, flooding caused by tsunami, and riverbank erosion studies; and the conceptual models are most suitable for probabilistic flood risk assessment, multi-scenario modelling, and water resources management on large floodplains.

Table 1 Comparative summary of the relative merits and weaknesses of different modelling approaches

METHOD	STRENGTHS	LIMITATIONS	SUITABILITY
Empirical models	Relatively quick and easy to implement Based on observation Derived inundation estimate is independent Technology is rapidly improving	Non-predictive No/indirect linkage to hydrology (difficult to use in scenario modelling) Coarse spatial and temporal resolution (although improving) Engineering limitations (sensors, carriers, transmission devices) Environmental impacts (clouds, wind, damaging weather conditions, other natural constrains) Processing errors (algorithm, artificial errors…)	Flood monitoring Flood damage assessment Serve as observations to support calibration, validation and data assimilation for other methods
Hydrodynamic models	Direct linkage to hydrology Detailed flood risk mapping Can account for hydraulic features/structures Quantifies timing and duration of inundation with high accuracy	High data requirements Computationally intensive Input errors can propagate in time	Flood risk assessment Flood damage assessment Real-time flood forecasting Flood related engineering Water resources planning River bank erosion Floodplain sediment transport Contaminant transport Floodplain ecology River system hydrology Catchment hydrology
Conceptual models	Computationally efficient	No inertia terms (not suitable for rapid varying flow) No/little flow dynamics representation	Flood risk assessment Water resources planning Floodplain ecology River system hydrology Catchment hydrology Scenario modelling

Source: adapted from Table 3 in (Teng et al., 2017))

3 Review of previous flood studies in MDB

The MDB extends across four States: New South Wales, Victoria, Queensland, and South Australia and covers an area of 1.061 million km^2. It is subject to multi-year droughts and intense wet periods. Mean annual precipitation across the Basin varies from around 200mm/year in the west to more than 1,500 mm/year in headwaters in the east. The basin has large interannual variability of precipitation and streamflow (Potter and Zhang, 2009), and the basin has seen statistically significant reductions in precipitation and streamflow in recent decades. The river system is also highly modified. River operators manage the river flows through a series of dams and weirs to provide water to irrigators and environmental assets along the length of the system. It is no surprise then, that there have been numerous flood studies by government agencies.

Government agencies ranging from the Commonwealth government organisations, State governments, CMAs, local councils, research institutes including universities and private organisations such as insurers, utility companies and consulting firms have carried out many flood modelling activities in the Basin throughout the years for various purposes. On one hand, this highlights the importance of the work; on the other hand, it is difficult to review all the previous work in details. Below are fifteen key flood inundation modelling reports, according to states and agencies and reviewed by the team, to gather insights from previous studies conducted across different parts of the Murray–Darling Basin in preparation for this project.

SA:

- 1956 flood model (Renmark Paringa - https://www.waterconnect.sa.gov.au/Content/Publications/DEW/DEWNR-TR-2015-56.pdf)
- Riverine Recovery Weir Pool Hydraulic Modelling Hydraulic Modelling (2012) - first database of flows (https://www.waterconnect.sa.gov.au/Content/Publications/DEW/Weir%20Pool%20Hydraulic%20Modelling_FINAL.pdf)
- 2020 Model (DHI) - updated database from SA
- Production of 80 000 ML/day flood inundation map for the South Australian section of River Murray (Montazeri & Gibbs, 2020)

(Some of the MIKE models are described separately – e.g. for Katarapko wetlands - https://www.waterconnect.sa.gov.au/Content/Publications/DEW/DEWNR-TN-2016-06.pdf)

NSW:

- Barwon Darling Reach 3 - Background document to the Floodplain Management Plan for the Barwon-Darling Valley Floodplain 2017 (https://www.industry.nsw.gov.au/__data/assets/pdf_file/0006/146085/Background-document-FMP-Barwon-Darling-Valley-Floodplain-2017.pdf)

- Mollee - Background document to the Floodplain Management Plan for the Lower Namoi Valley (2020) (https://www.industry.nsw.gov.au/__data/assets/pdf_file/0011/321131/Background-document-to-the-Floodplain-Management-Plan-for-the-Lower-Namoi-Valley-Floodplain-2020.pdf)
- Lower Gingham (report not publicly available)
- Murrumbidgee
- Macquarie Marshes

CSIRO:

- Darling system (Dutta et al., 2016)
- Edward-Wakool system (Vaze et al., 2018a)
- RiM-FIM (Penton et al. 2007, Sims et al., 2014)
- MDB-FIM (Chen et al., 2011)

MDBA:

- Lindsay hydraulic model (Water Technology 2006)
- Edward Wakool Model (currently under development)

After examining the above-mentioned models and reports, five large-scale high impact projects that have accessible modelling results were selected (Table 2).Their spatial locations are shown in Figure 1.

Table 2 Selected flood modelling projects in MDB

LOCATION	ORGANISATION	PURPOSE	MODEL	MORE INFORMATION
The South Australian section of River Murray	SA Department for Environment and Water	Environmental flow	MIKE FLOOD	(Montazeri and Gibbs, 2020)
Lower Balonne and Middle Darling System	CSIRO MDBA	Water management Environmental flow	MIKE 21	(Dutta et al., 2016)
Lower Murrumbidgee River	CSIRO NSW Office of Environment and Heritage	Environmental flow Flood risk management	RiM-FIM TUFLOW (upstream of Balranald)	(Sims et al., 2014) (Burke et al., 2022; Tetley, 2022; Wells and Streeton, 2022)
Namoi River	NSW Office of Environment and Heritage	Healthy floodplains and general flood studies and investigations	MIKE 11 MIKE 21 Flexible Mesh (FM) MIKE FLOOD FM	(NSW OEH, 2017)
Edward-Wakool System	CSIRO MDBA	Water management Environmental flow	RiM-FIM MIKE 11 MIKE 21	(Sims et al., 2014)

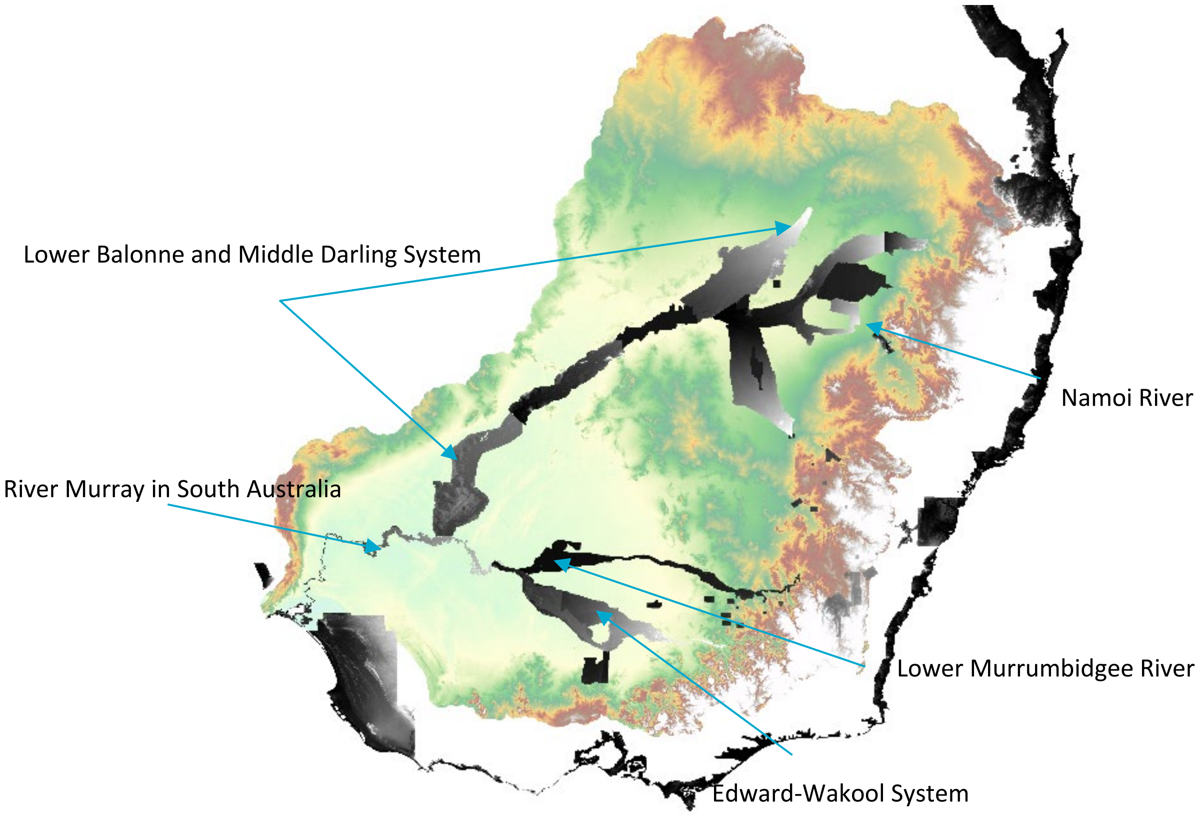

Figure 1 Spatial location of a number of selected flood modelling projects

4 Input data preparation

High-quality data is essential for building a robust model. As a critical component of model development, several input datasets were compiled during the initial phase of the research, with continuous improvements made throughout the project. These datasets were fundamental to the development and validation of the RQ7 model. The datasets are accessible through the CSIRO Data Access Portal (https://data.csiro.au/). This section provides detailed descriptions of the datasets, which include the digital elevation model (DEM), hydrodynamic modelling results, gauged data, soil property data, and climate data.

4.1 DEMs

4.1.1 DEM fusion

This section is adapted from Gallant (2019).

Modelling of flood inundation requires accurate topographic data, which in most cases means a high-resolution LiDAR or photogrammetric DEM with removal of non-ground features like vegetation. The entire modelling domain must be represented but the area prone to flooding is often a small part of the entire domain, therefore it is often cost-effective to use expensive and detailed elevation data in the focus area and cheaper, less detailed data elsewhere. This leads to the need for combining the two DEMs seamlessly so that there are no abrupt changes in height or slope at the transition.

In the MDB, LiDAR data was collected in the floodplain area covering most part of floodplains along the main river channels (Figure 2) and the remaining area was covered by SRTM-derived DEM-H at 1 arcsecond resolution. We have adopted a method first developed by (Gallant, 2019) for adjusting the DEM-H to match the LiDAR data to remove abrupt steps at the boundary to ensure the combined data are suitable for flood modelling. Two main steps in the process are (1) removal of systematic vertical errors and (2) adjusting the less reliable DEM-H to match the LiDAR at the boundary. We have improved the method by fine-tuning the buffer size at the boundary of the two DEMs. The method successfully removed local steps and produced a satisfactory result as shown in Figure 2 (Marvanek et al., 2022).

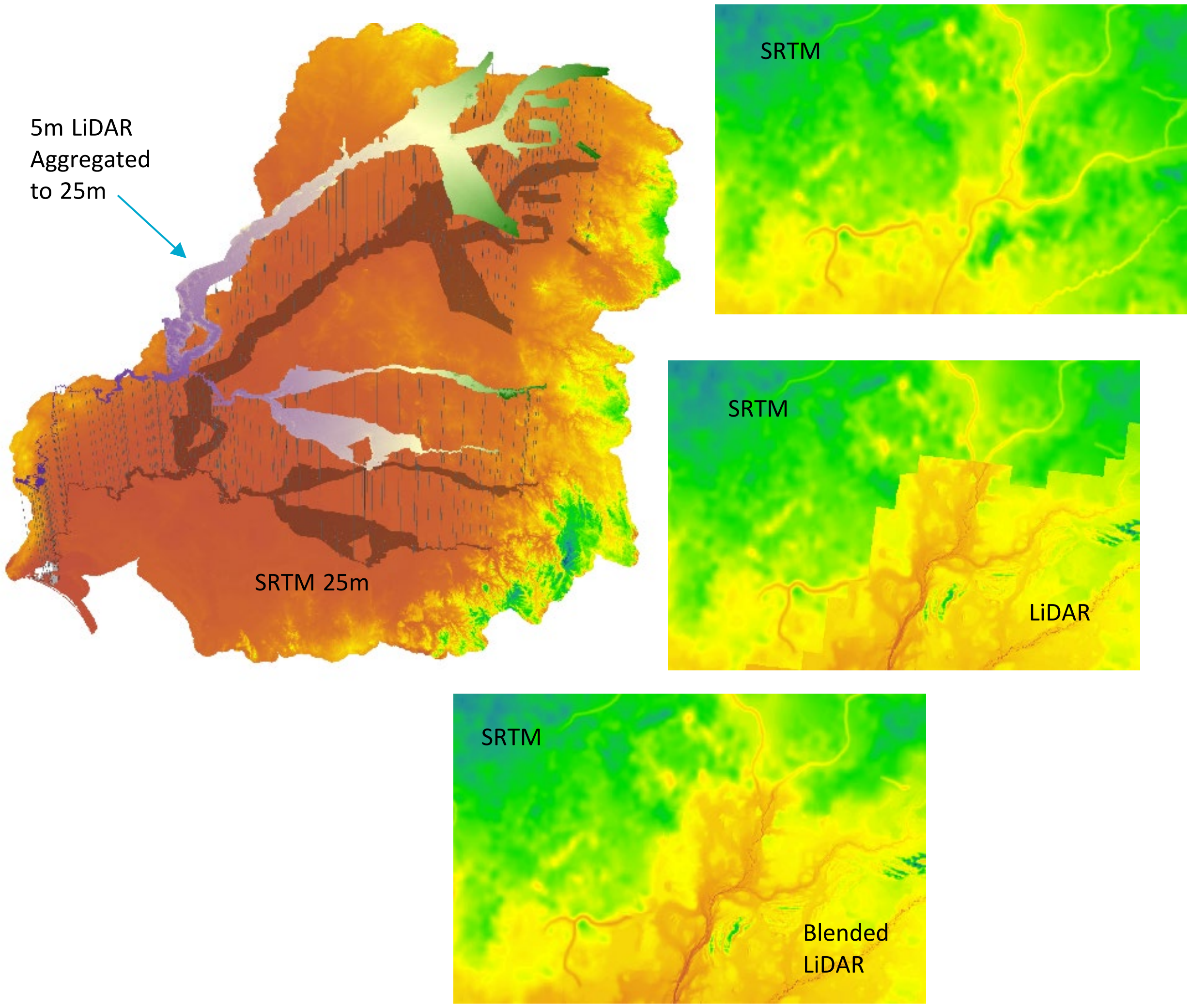

Figure 2 Merging LiDAR DEM and SRTM: the original SRTM and LiDAR DEM are shown in the large map on the left; the top right insert shows a zoomed in view of SRTM; the middle insert shows the abrupt change (local steps) at the boundary of the two datasets; the bottom insert shows the merged data with the abrupt change removed.

4.1.2 Latest version of DEM

As new DEM datasets are gradually becoming available, we have set up a strategic project in CSIRO to investigate better methods (including methods using AI/ML) to merge different datasets, including SRTM, LiDAR, and Photogrammetry data. We have used the outcome from the strategic project to update the DEM whenever a new dataset becomes available.

The Digital Elevation Model (DEM) is crucial for flood inundation modelling, as the terrain significantly influences water movement. While an optimal choice is a high-resolution Light Detection and Ranging (LiDAR) DEM, its availability is limited across the Murray-Darling Basin (MDB). Marvanek et al. (2022) adopted a methodology initially developed by Gallant (2019) to merge and gap-fill LiDAR DEM with a global DEM. This method involves adjusting the global DEM to align with LiDAR data, eliminating abrupt steps at the boundary and ensuring the combined data are suitable for flood modelling.

Based on feedback from downstream researchers and data users, we have identified the need for an improved DEM to enhance the precision of our floodwater depth estimates. Funded by CSIRO Environment, the Digital Water and Landscapes (DWL) initiative has generated a Basin-wide DEM using the Gallant (2019) method and latest Elvis (fsdf.org.au) data (up to November 2022), making it more recent and accurate. Collaborating with DWL and the MDBA, we are actively working to establish bathymetry data for channels and large lakes, intending to integrate bathymetry data seamlessly into the DEM.

In the pre-processing for the MDB DEM, all the original input DEMs (as seen in different colours in Figure 3) were bilinearly resampled to 5 m, reprojected to the GA LCC projection (EPSG 7845; datum GDA2020), and adjusted to the Australian Vertical Working Surface vertical datum (AVWS, which is more accurate over 100s of kilometres than the Australian Height Datum). The “gap filling” DEM is the FABDEM (Forest and Buildings removed Copernicus DEM; Hawker et al. 2022), which is a global elevation map that removes building and tree height biases from the Copernicus GLO 30 DEM with 30 m resolution.

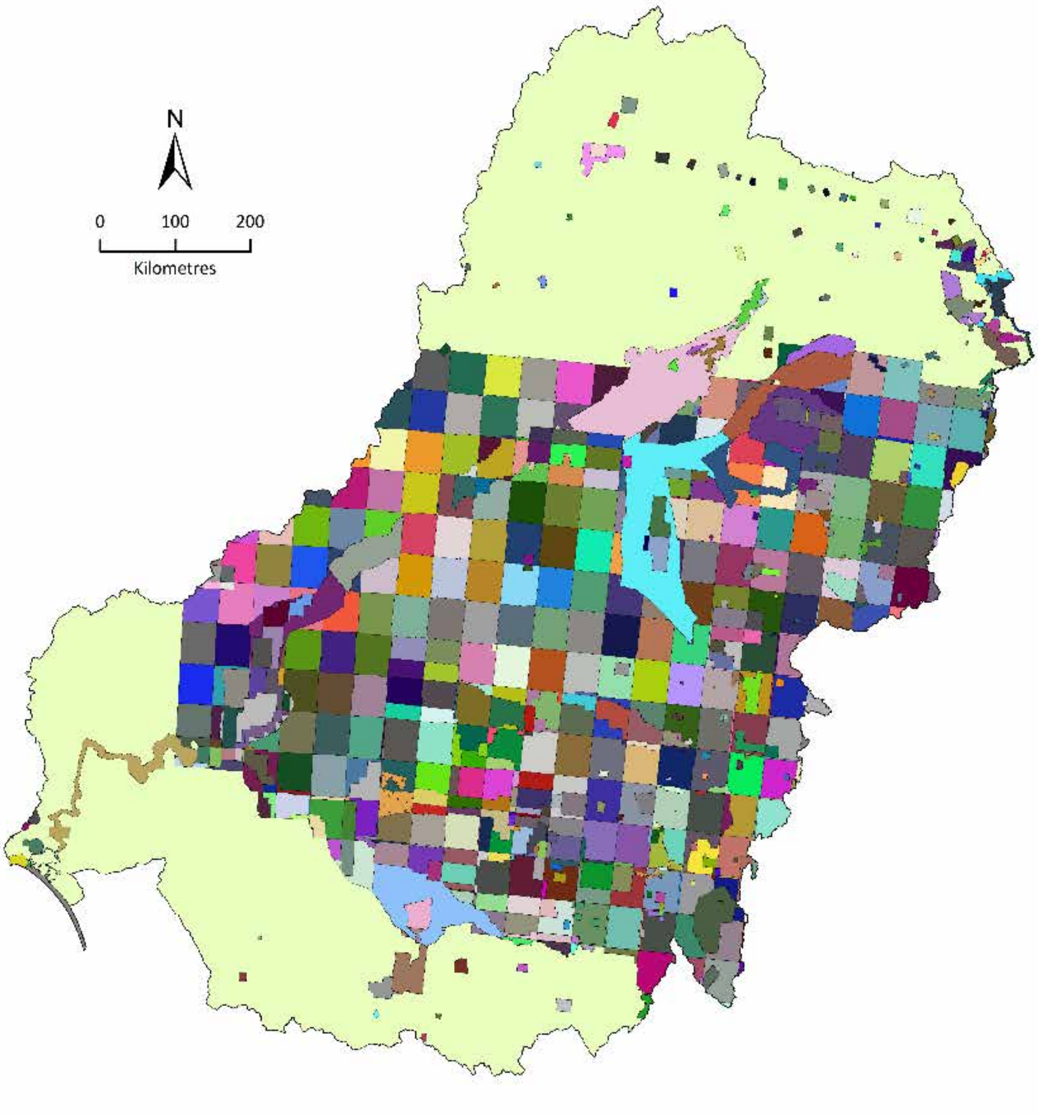

Figure 3 Input DEMs from Elvis that were merged into the new version of the basin-wide DEM.

The method from Gallant (2019) was adapted to merge the DEMs. For merges involving two LiDAR DEMs (or original grid cell resolution of 2 m or less), two gaussian smoothing steps were used. For merges where the coarser of the pair of DEMs had a 5 m original grid cell resolution, 4 gaussian smoothing steps were used, and for merges where the coarser DEM had an original grid cell resolution of 10 m or more, 8 gaussian smoothing steps were used. More gaussian smoothing steps increased the distance over which the difference between the datasets was added to the coarser DEM, with 1 x the difference added at the edge, tapering to 0 x the difference at the gaussian-step-defined distance from the edge. Figure 4 illustrates the steps required to create and quality assure the new version of the basin-wide DEM.

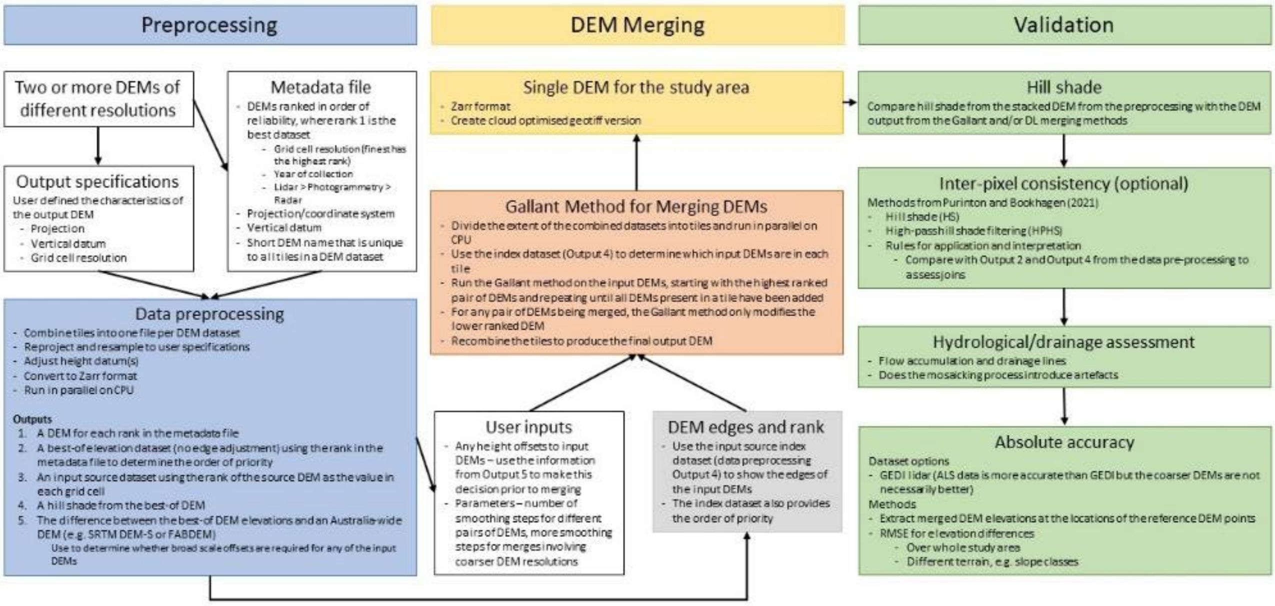

Figure 4 Flow chart of the processing steps for generating the new version of the basin-wide DEM.

4.1.3 Integrating bathymetry into the DEM

One of the known weaknesses of the MDB maximum two-monthly water depth data was the less accurate water depth estimation for permanent water bodies, including main river channels and large lakes. The main reason for these errors is the presence of water during the capture of DEM data. To address this issue, integrating bathymetry data into the DEM is necessary, to include the structure below the water surface. In collaboration with DWL, we identified, collated, and processed existing bathymetric datasets for the MDB from multiple sources and produced a consistent MDB bathymetrically enforced elevation dataset.

There is no current technology that calculates the elevation of land under permanently wet rivers and dams due to the likely presence of suspended sediments and aquatic vegetation. Bathymetric LiDAR uses a green light sensor however very clear water is essential for consistent and accurate data collection. For permanently wet rivers, lakes and dams, methods such as traditional surveying and sonar acquisitions from boats are required. Different types of bathymetry data exist from various sources and were developed for different purposes. Figure 5 shows the distribution and types of input bathymetry data. Figure 6 illustrates types of the raw point data bathymetry that we have acquired, and gaps presented in the data.

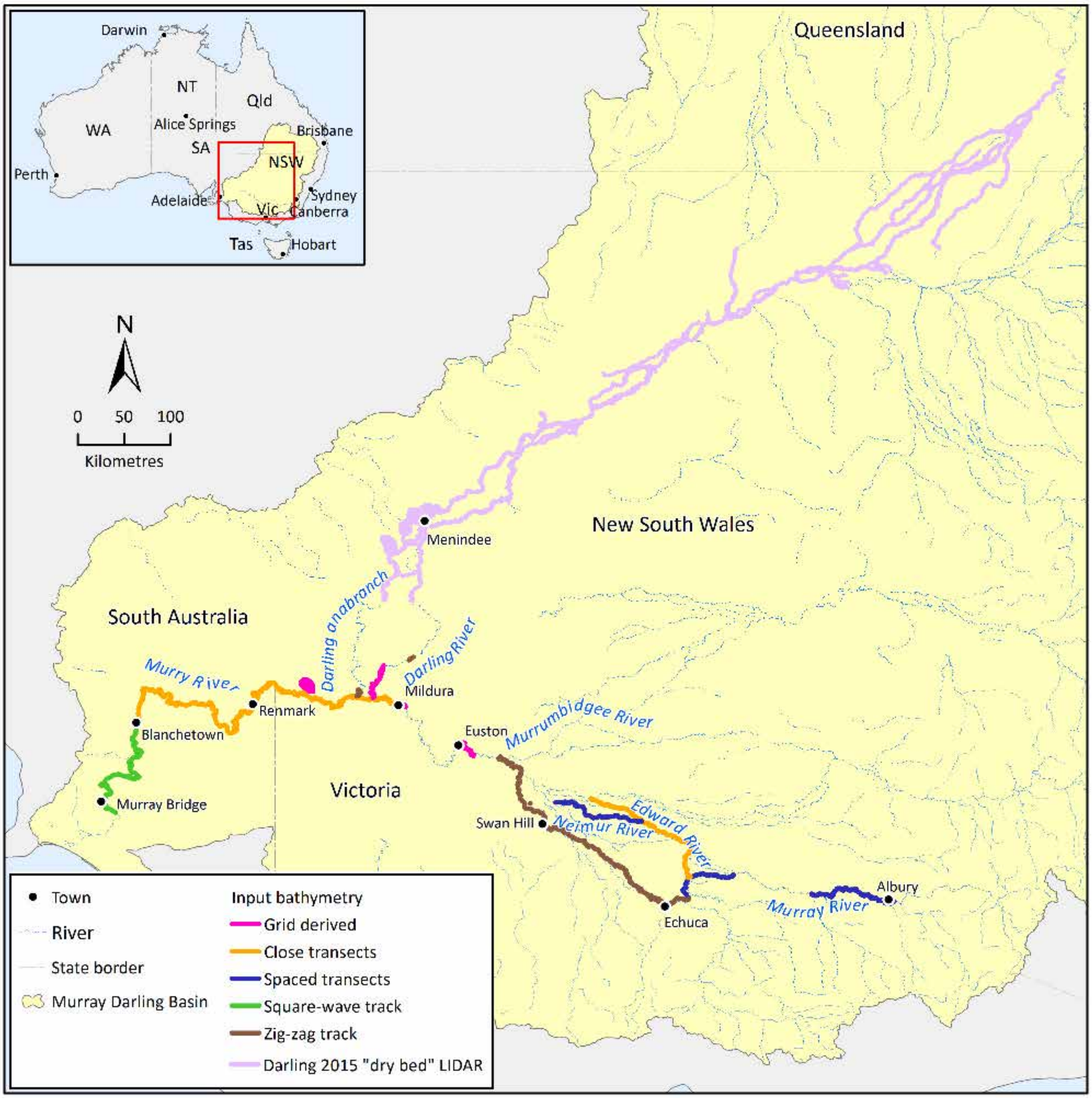

Figure 5 Map showing different types of input bathymetry data.

Bathymetry point data were received for large sections of the Murray River (Hume to Wellington) (see Figure 5) as well as sections of the Darling Anabranches and the Edward River. Some small sections were clearly derived from gridded bathymetry having dense regular spacing of 10 to 15m. Most of the points were a continuous line of points following either a zig-zag or square wave track, with the remainder being transects perpendicular to the riverbanks at regular intervals ranging from a few hundred metres to many kilometres apart. Coverage for the Murray downstream of Lake Hume was continuous in some form (grid, track or transect) save for gaps between Narrung and Mildura. Various techniques were developed to process these data to form a consistent bathymetry ready to be enforced into the new version of the DEM.

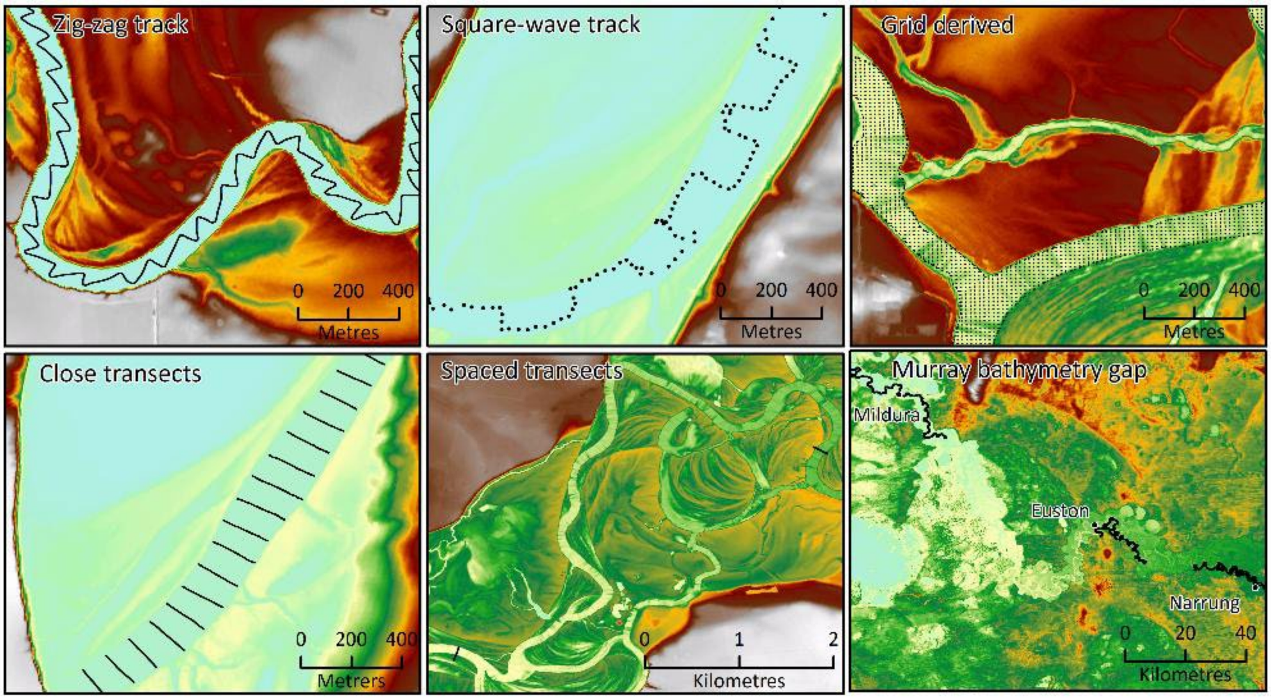

Figure 6 The raw point data bathymetry came in types: zig-zag track (upper left), square wave (upper middle), grid derived (upper right), close transects (lower left), spaced transects (lower middle) as shown above. The point datasets (black dots) are shown on top of the elevation, which is shown on a relative scale of dark brown (higher) to light blue (lower). The gaps in the data (e.g. along Murray River as shown in lower right panel) were filled with interpolated data based on the nearest transects.

Grid derived points were interpolated directly to a 5m grid conforming to the DEM using Triangular Irregular Network (TIN) in ArcGIS. The remaining point configurations were unsuitable for direct interpolation to a DEM conforming raster in their received form, and so underwent a data point densification process to make them suitable.

Figure 7 illustrates the method developed by Steve Marvanek to form gridded bathymetry from observed data points through data point densification. This was achieved by first creating a dense regular array of points consisting of 30 to 40 files of closely spaced (~10-~20m) points across the width of the channel and following the course of the channel.

Input bathymetry point data was transferred to its nearest (within 5m to 20m search radius) array point. Intervening array points within a given file that had not inherited a close neighbouring bathymetry datapoint value, then had a value linearly interpolated from its next upstream and downstream value.

Bathymetry data points (black) confer their bathymetry value to nearby array points (red). Remaining array points (blue) then have an interpolated value calculated based on the upstream and downstream conferred data in their file. This dense array of data was then interpolated to the DEM conforming 5m raster using TIN. The rasterised bathymetry data were then inserted into the DEM replacing the non-ground channel values with bathymetry values.

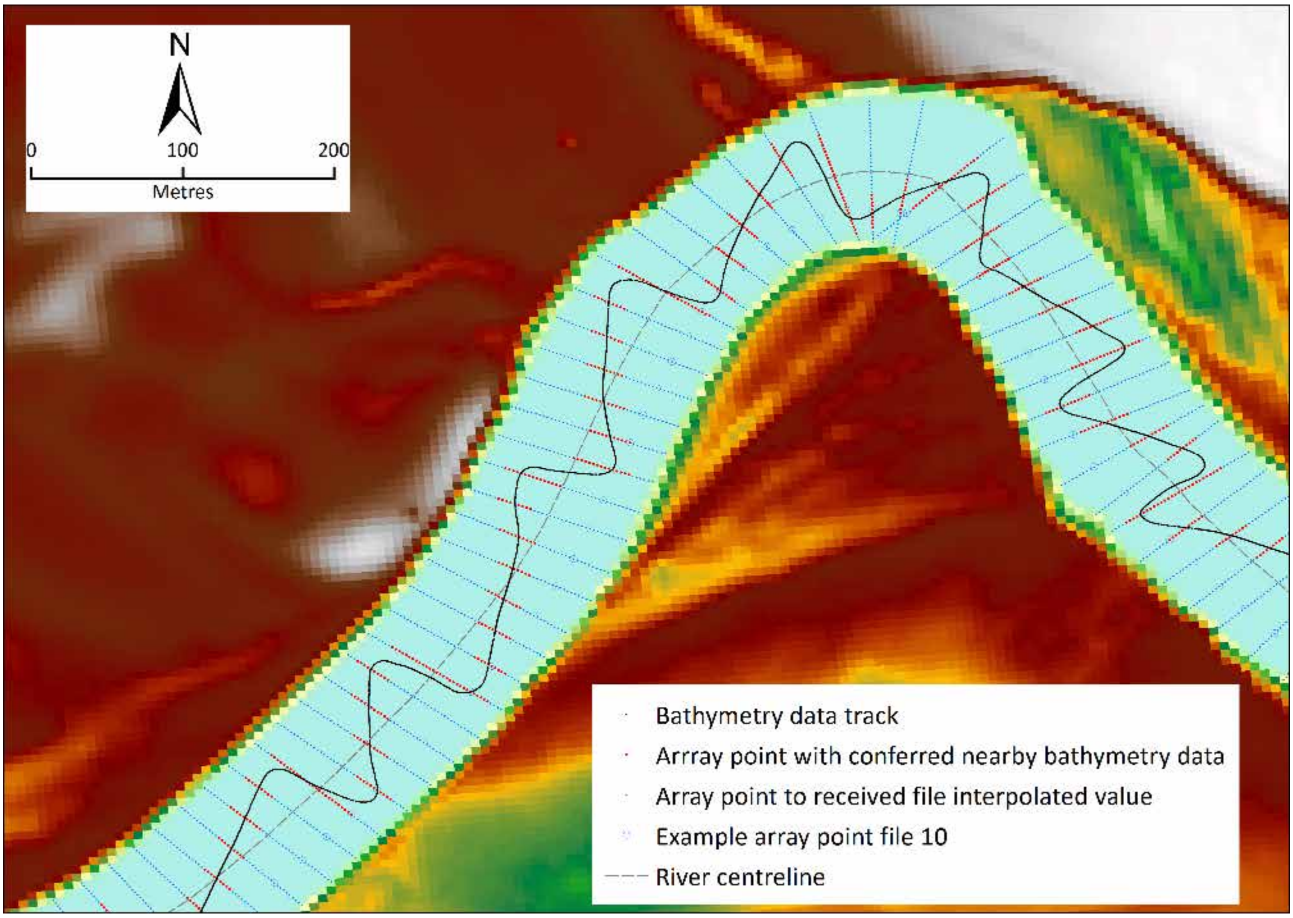

Figure 7 Illustration of the method that processes the zig-zag track height observations (black) to form bathymetry. The bathymetry data points (black) confer their bathymetry value to nearby array points (red). Remaining array points (blue) then have an interpolated value calculated based on the upstream and downstream conferred data in their file.

4.2 Hydrodynamic modelling results

The RQ7 newly proposed model's predicted water depth will need to be validated with 'true' water depth across the floodplain. As the water depth observations on floodplain are rare and difficult to obtain, for the purposes of the validation, we will be limited by mainly using the depth predicted by a hydrodynamic model as 'true' water depth. Although there are many previous hydrodynamic modelling experiments carried out in the MDB, only a few of them have the datasets available in the format and quality that can be used for the purpose of the RQ7 research. For the comparison to be meaningful, it was essential for the hydrodynamic model to be of the highest standard. The RQ7 project evaluated hydrodynamic models based on:

- whether they were peer reviewed, especially whether they had been revised and improved based on experience or feedback.
- whether they were calibrated to dynamic conditions (as distinct from steady-state models).
- the quality of DEM and channel bathymetry – only those based on high resolution LIDAR digital terrain models were considered.

- the resolution of the floodplain in the modelling, with preference to flexible meshes.
- consistency with other information such as gauged levels and spot heights.

The project identified models that best met these criteria – three of which would be used in an initial assessment of model accuracy and an additional two that would be acquired for later analysis. For the initial three models, we extracted outputs of model depth for calibration events to use as validation datasets. This dataset encompassed three locations in the MDB, 11 river reaches and seven calibration events.

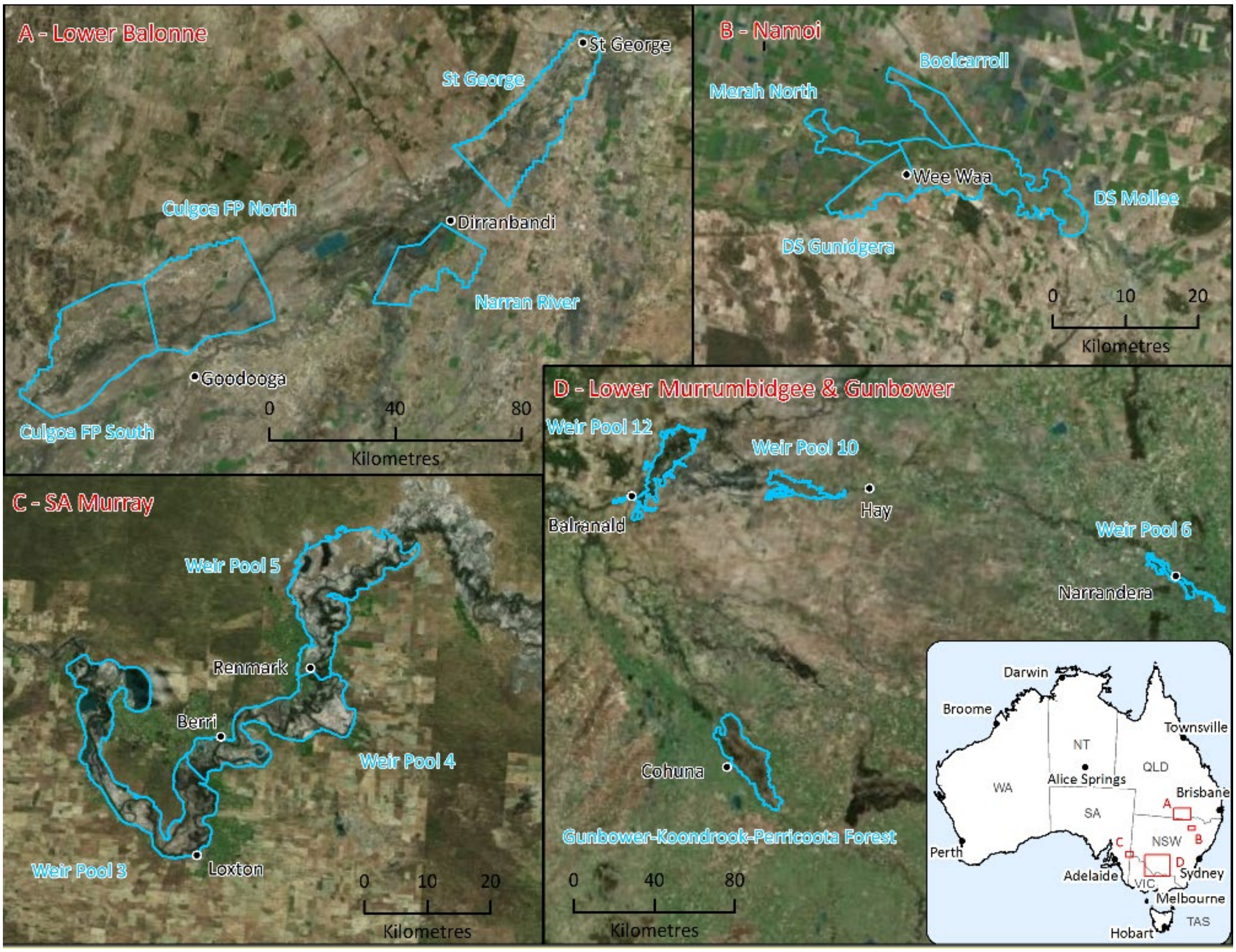

Figure 8 The locations for the available validation datasets including A. The Lower Balonne River; B. Namoi River; C. Murray River in South Australia; and D. three reaches of the Murrumbidgee River.

As shown in Figure 8 the first location (A) covered the area of the Balonne River downstream of the St George township in Queensland to Weilmoringle in New South Wales. The Culgoa River is an upper tributary of the Darling River in the far north-west of the MDB. The second location (B) was the Namoi River from Keepit Dam to the junction of the Barwon River near Walgett in New South Wales (one of the upper tributaries of the River Murray). The third location (C) was between Lyrup and Lock 3 on the River Murray in South Australia. The forth location (D) was the middle reaches of the River Murray (around Gunbower-Koondrook Perricoota forests) and lower reaches of the Murrumbidgee River (near the townships of Narrandera, Hay and Balranald). The locations were broken down into reaches based upon the location of streamflow gauges and water infrastructure, location of major confluences or distributaries, and location of major irrigation districts. As a result, the Balonne study location was broken into four reaches, the Namoi study area was broken into four reaches and the SA study location was broken into three reaches.

Table 3 describes the hydrodynamic models for the Balonne, Namoi and Lower River Murray. In total there were seven flood events spread across the three study locations with peak discharges of around 25 GL/d to 300 GL/d.

Table 3 Hydrodynamic model properties of Balonne, Namoi and Lower Murray

	BALONNE RIVER	NAMOI RIVER	LOWER-RIVER MURRAY
Shortened form in graphs	LBS (Lower Balonne System)	Namoi	SA (South Australia)
Jurisdiction	Queensland, New South Wales	New South Wales	South Australia
Model Type	MIKE 21 – 90m Grid	MIKE 21 Flexible Mesh (FM)	MIKE HYDRO River for channel, MIKE 21 Flexible Mesh for floodplain
Dynamic/steady	Dynamic	Dynamic	Dynamic for 25 GL/d, steady state for 90 GL/d
Flood discharge (nominal)	150 GL/d, 50 GL/d, 250 GL/d, 300 GL/d	185 GL/d	25 GL/d, 90 GL/d
Dates modelled	1995-12-27 to 1996-01-30 2008-01-19 to 2008-02-23 2010-12-28 to 2011-01-28 2012-01-28 to 2012-03-02	1998-07-20 to 1998-07-31	2013-09-06 to 2013-11-03 2016-12-09
Gauging station used for measurement	Balonne at St George (422201),	Namoi River at Molle (419039)	Lock 1 U/S (A4260902) and Calculate for to South Australia (A4261001)
Dates of imagery used	1996-01-28, 2008-02-05* (filled with imagery from: 02-22, 01-29, 02-06), 2011-01-21, 2012-02-17	1998-07-24 (Aerial photography)	2013-10-30, 2016-12-09 (filled with imagery from 2016-12-25)
Publications	Dutta et al, 2016	(NSW OEH, 2017)	Montazeri and Gibbs, 2020
Notes	There are significant irrigation districts in the area (e.g. Cubbie station). We have defined the reaches to avoid these areas.	LandSat imagery was not available for this flood. The channel was defined using cross-sections.	The bathymetry of some small permanent lakes were not fully incorporated in model.

Source: Teng et al. (2022)

Table 4 describes the hydrodynamic modellings for the lower Murrumbidgee River and the middle reaches of the River Murray.

Table 4. Hydrodynamic model properties of Gunbower and Lower Murrumbidgee

	LOWER MURRUMBIDGEE RIVER	MID-RIVER MURRAY RIVER
Shortened form in graphs	Bidgee	Gunbower
Jurisdiction	New South Wales	New South Wales, Victoria
Model Type	TUFLOW 1D + 2D One model for each of Weir Pool 6, 10 and 11	MIKE HYDRO River for channel, MIKE 21 Flexible Mesh for floodplain
Dynamic/steady	Dynamic	Dynamic
Flood discharge (nominal)		
Dates modelled	Weir Pool 6: 2021-06-13 (warm up from 2021-06-06) to 2021-08-26 Weir Pool 10: 1992-10-06 to 1992-11-27; 2021-07-10 to 2021-09-11 Weir Pool 12: 2017-11-20 to 2017-12-21; 2021-06-24 to 2021-10-01; 2010-10-15 to 2011-02-09; 2016-05-10 to 2016-08-29	2016-09-17 to 2016-10-22
Gauging station used for measurement	Weir Pool 6: Murrumbidgee River at Narrandera (410005); Yanco Creek at Offtake (410007); Murrumbidgee D/S Yanco Weir (410036) Weir Pool 10: D/S Hay Weir (410136); D/S Maude Weir (410040); Maude Storage (41010941); Nimmie Storage (41010287) Weir Pool 12: Murrumbidgee D/S Maude Weir (410040); Murrumbidgee D/S Redbank Weir (410041); Redbank Storage (41010966); and Murrumbidgee D/S Balranald Weir (410130)	Murray River at Torrumbarry (409207);
Publications	Burke et al., (2022); Tetley (2022); Wells and Streeton (2022)	
Notes		At time of publication not all information about this model was available

4.3 Gauged flow, water level and cross section

The gauged flow and water level data are needed to relate flow and water level for interpolation and model simulation. The velocity data are required to estimate the travel time for each modelling reach, which is essential to determine the size of modelling regions. Velocity u can be derived from

$$u = \frac{Q}{A} \quad (1)$$

where Q is flow (in m^3/sec or ML/day), A is cross section area, which is a function of water level.

Table 5 lists the online data portals that can be used to extract MDB gauged water data observations and gauge information. The quality assurance of the data presented some challenges, particularly in determining whether the gauged water levels are referenced to local level datum or AHD elevations. To address this, we have collaborated with MDBA to obtain operational data wherever available. Additionally, we have reached out to State governments to request data along with the associated metadata. We have also accessed a snapshot of datasets from previous projects where licenses have been granted, such as the AWRA and MDB-EF projects. This has been an iterative process, adapting to changing requirements and incorporating new data as it becomes available, involving close coordination with data custodians and tasks such as manual extraction, digitization, and other data processing efforts. The compiled dataset has been used by the team for the purpose of this project but has not been published due to licensing restrictions.

Table 5 Online water data portals

NAME	WEB SITE	PROVIDER	DATA COVERAGE
Water Data Online	http://www.bom.gov.au/waterdata/	Bureau of Meteorology (BoM)	Nation-wide
The River Murray system Live river data	https://riverdata.mdba.gov.au/system-view/	MDBA	The River Murray System
WaterNSW	https://realtimedata.waternsw.com.au/	NSW government	NSW
Water Data SA	https://water.data.sa.gov.au/	SA Department for environment and water	SA
Water Measurement Information System VIC	https://data.water.vic.gov.au/	VIC Department of environment, land, water & planning	VIC
Water monitoring information portal	https://water-monitoring.information.qld.gov.au/	QLD government	QLD
ALS client data portal	https://hydportal.alsglobal.com/web.htm	ACT Icon Water/ACT gov	ACT

4.4 Soil property data

The soil property data are required for estimating infiltration in the model simulation as described in Section 2.1.4. We have obtained the soil property data, namely, saturated hydraulic conductivity for the top soil layer (0 – 10 cm), shallow soil layer (10 – 100 cm) and deep soil layer (100 – 600 cm), available water holding capacity for the top soil layer (0 – 10 cm), shallow soil layer (10 – 100 cm) and deep soil layer (100 – 600 cm) from the Australian Water Resource Assessment Landscape Model (AWRA-L). The nation-wide data layers at 90 m resolution, which was aggregated to 1 km and 5 km resolutions to support AWRA-L, will be extracted for modelling regions to estimate amount of water lost to infiltration for each grid cell at each time step. The methodology for estimating soil hydraulic properties grids using pedotransfer functions and digital soil mapping is described in Appendix A in (Vaze et al., 2018). Vaze et al. (2018b) also provides a brief description of each of the spatial layers (including the source data used to derive the layers) that are used in the continental AWRA-L implementation.

4.5 Climate data

For the historical period, daily rainfall of each grid cell was sourced from the SILO gridded dataset (Jeffrey et al., 2001), and potential evapotranspiration was calculated from the SILO climate surfaces using Morton's wet environment algorithms (Chiew and McMahon, 1991; Morton, 1983). Future rainfall projections were generated using the Daily Scaling method (Chiew et al., 2009), informed by climate change signals from 37 CMIP6 GCMs for Shared Socioeconomic Pathway 5-8.5 (SSP5-8.5) (for a 30-year time slice centred on 2060 relative to a 30-year time slice centred on 1990, representing approximately 2.3°C average global warming) (Zheng et al., 2024). The daily scaling method perturbs historical climate time series data based on the change signals derived from GCMs, reflecting changes in both the means and the shape of the daily rainfall distribution, which is important for capturing the intensification of extreme rainfall simulated by GCMs. Future potential evapotranspiration was generated using the seasonal scaling method (Chiew et al., 2009), which was also informed by the corresponding CMIP6 GCMs.

Part II Research

1 Introduction

This chapter details the research conducted under RQ7 to advance our understanding and modelling capabilities of floodplain inundation across the Murray–Darling Basin (MDB). One of our primary focuses has been to improve the accuracy of surface water detection from satellite imagery, utilizing data from high-resolution sources, particularly Landsat and Sentinel-2. These efforts have enhanced our ability to monitor water dynamics over vast areas, laying the foundation for more precise and robust floodplain modelling. In addition, we benchmarked water depth estimation models, ensuring that the derived measurements align with the results from hydrodynamic models, which has been crucial for accurate depth and volume estimations across the floodplain.

The findings from such research have led to the creation of extensive, basin-wide datasets and the development of the RQ7 model. The floodplain inundation extent and water depth datasets provide an unprecedented opportunity to quantify essential inundation characteristics, including trends, inter- and intra-annual variability, and other critical metrics. They allow us to link floodplain inundation patterns with both current and projected climate scenarios. This research has significantly enhanced our understanding of how future climate changes may impact floodplain dynamics, especially regarding the frequency and intensity of inundation events.

Moreover, we developed a floodplain ecological response model to utilise the inundation data generated by the RQ7 model. This ecological model quantifies the responses of floodplain ecosystems, with a particular focus on vegetation dynamics. By linking inundation characteristics to ecological outcomes, the response model provides a valuable tool for predicting and understanding the environmental impacts of flooding. This work supports resource managers and policymakers in making informed decisions regarding environmental water allocations, enabling more adaptive and sustainable floodplain management strategies under varying climate conditions.

Here we provide a comprehensive overview of the research approaches, methodologies, and findings that underpin the RQ7 model and its associated datasets, highlighting the project's contributions to floodplain inundation science and environmental management in the MDB.

2 Surface water detection from satellite imagery

Accurately mapping surface water extent is critical in estimating water volume and monitoring changes for effective water management. This is essential for human consumption, agricultural use, and maintaining the ecological health of wetlands and rivers. With a growing population and changing climate, the need for precise information on available water is more critical than ever, especially in Australia, which is the driest inhabited continent in the world and continues to experience large interannual variability between dry and wet periods.

Ground observations of surface water extent can provide valuable information but are not always available, and large-scale synopses of current and historical water extent through gauging stations and high-water marks are hard to obtain. Remote sensing technologies offer an affordable means of capturing surface water extent with reasonable spatial and temporal coverage suitable for water monitoring. The Landsat satellite series' spatial resolution (30m) makes it suitable for capturing (subject to cloud cover) much of the fine spatial detail of a large river basin. The Landsat archive provides data dating back to 1987 for the thematic mapper series. Each Landsat satellite returns to the same point every 16 days. Given there can be overlap in the operation of one satellite with its replacement, the temporal frequency varies through history and can be greater than 16 days.

The Water Observations from Space (WOfS) dataset is generated by Geoscience Australia and available through Digital Earth Australia (Mueller et al., 2016). WOfS uses a decision tree approach based on a selection of Landsat spectral bands and indices, as well as ancillary products (including topography and hydrology layers) to constrain water extent to likely areas. Individual WOfS images of surface water extent, along with summary statistics from the 1980s to the present, are available for Australia for the entire Landsat archive. WOfS provides a conservative estimate of surface water extent, making it a robust product, but it is more likely to underestimate than overestimate water extent (Sims et al., 2018).

To address the challenge associated with the surface water detection from satellite imagery, we assessed the performance of various commonly used indices across different environments. Based on our findings, we developed a Multi-Index Method (MIM) for detecting surface water from Landsat imagery. To extend its applicability to Sentinel-2 data, we recalibrated the MIM to account for differences between the two satellite platforms. Additionally, we explored methods to optimize spatial alignment between the Landsat MIM and Sentinel-2 MIM, ensuring a seamless and consistent water extent product. Significant effort was also dedicated to enhancing the MIM's performance in wetlands and densely vegetated areas. These advancements are detailed in the following sections.

2.1 Development of Multi-Index Method (MIM) surface water detection algorithm

This section is adapted from Ticehurst et al. (2022).

A multi-index method (MIM) has been developed for mapping surface water extent within the Murray-Darling Basin (Ticehurst et al., 2022). It is based on existing indices, such as the modified Normalised Difference Water Index (mNDWI; Xu, 2006), Fisher's water index (FWI; Fisher et al., 2016), and the Tasseled Cap Wetness Index (TCW; (Dunn et al., 2019), which are already used for mapping surface water extent. Each index is applied in the area where it performs best, and the resulting rule-set uses NDWI>–0.3 to map water in major perennial rivers, TCW>-0.035 to map water in wetlands, and the maximum of NDWI>0 and FWI>0.63 for mapping water in the remaining areas. Based on 440 validation plots in the Murray-Darling Basin, this resulted in an overall balanced accuracy of 93% (Table 6).

Table 6 Accuracy of various indices.

Water Index	Balanced accuracy
MIM	93%
Fisher WI	91%
mNDWI>0	91%
mNDWI>-0.3	90%
TCW >-0.035	92%
TCW >-0.01	90%
WOFS	86%

Using the water index with the best performance for the different water environments (i.e., ‘Major Perennial Rivers’, ‘Wetlands’, ‘Large Water Storage’, and ‘Remaining plots with water’) within the MDB, the MIM was used for mapping surface water across the basin (Figure 9 with the Landsat bands needed from DEA are the red, green, blue, near infrared, the two shortwave infrared bands, and the cloud mask band-fmask). This multi-index method uses the following set of rules:

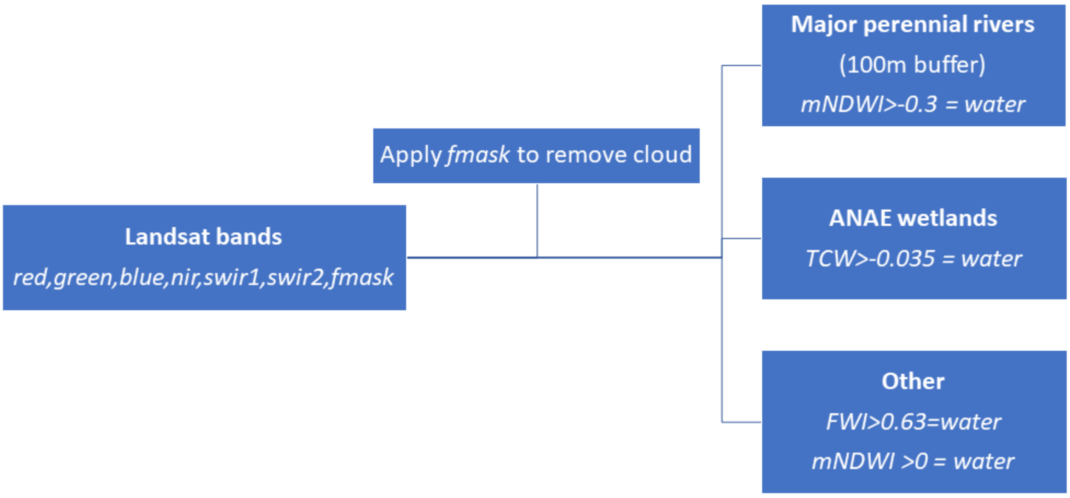

Figure 9 (Figure 3 from Ticehurst et al., 2022). Multi-Index method developed for mapping surface water across the Murray Darling Basin (SWIR1 and SWIR2 = shortwave infrared bands, fmask = Landsat cloud mask, mNDWI = modified Normalised Difference Vegetation Index, TCW = Tasseled Cap Wetness index).

The original combined MIM and WOfS surface water extent datasets were produced to cover the entire MDB from 1988 to 2022. The latest dataset (from 1988 to June 2024) can be used to explore long-term and seasonal trends across the basin as well as any area of interest within the basin.

2.2 Incorporating Sentinel-2 data

In preparation for generating the new version of the floodwater depth data, we have incorporated the Sentinel-2 imagery to enhance the surface water detection via improvements to the original Multi-index Method (MIM) (Ticehurst et al., 2022).

To maximise detection of water as well as ensure the best spatial match between the Landsat MIM and Sentinel-2 MIM to create a seamless water extent product, different data-loading and resampling methods have been investigated. Enforcing the corner coordinates of the bounding box to be the same in both Landsat and Sentinel-2 proved to be better than using the generic data-load option. While the bilinear resampling method showed the smallest difference between the Landsat and Sentinel-2 data, it was unable to detect the same finer water features that the nearest neighbour resampling method could. Hence the nearest neighbour resampling method was used. Figure 10 below shows how the different resampling methods influence the detection of water in the Landsat and Sentinel-2 modified Normalised Difference Water Index. The histogram shows that the bilinear resampling method has the smallest difference between Landsat and Sentinel-2.

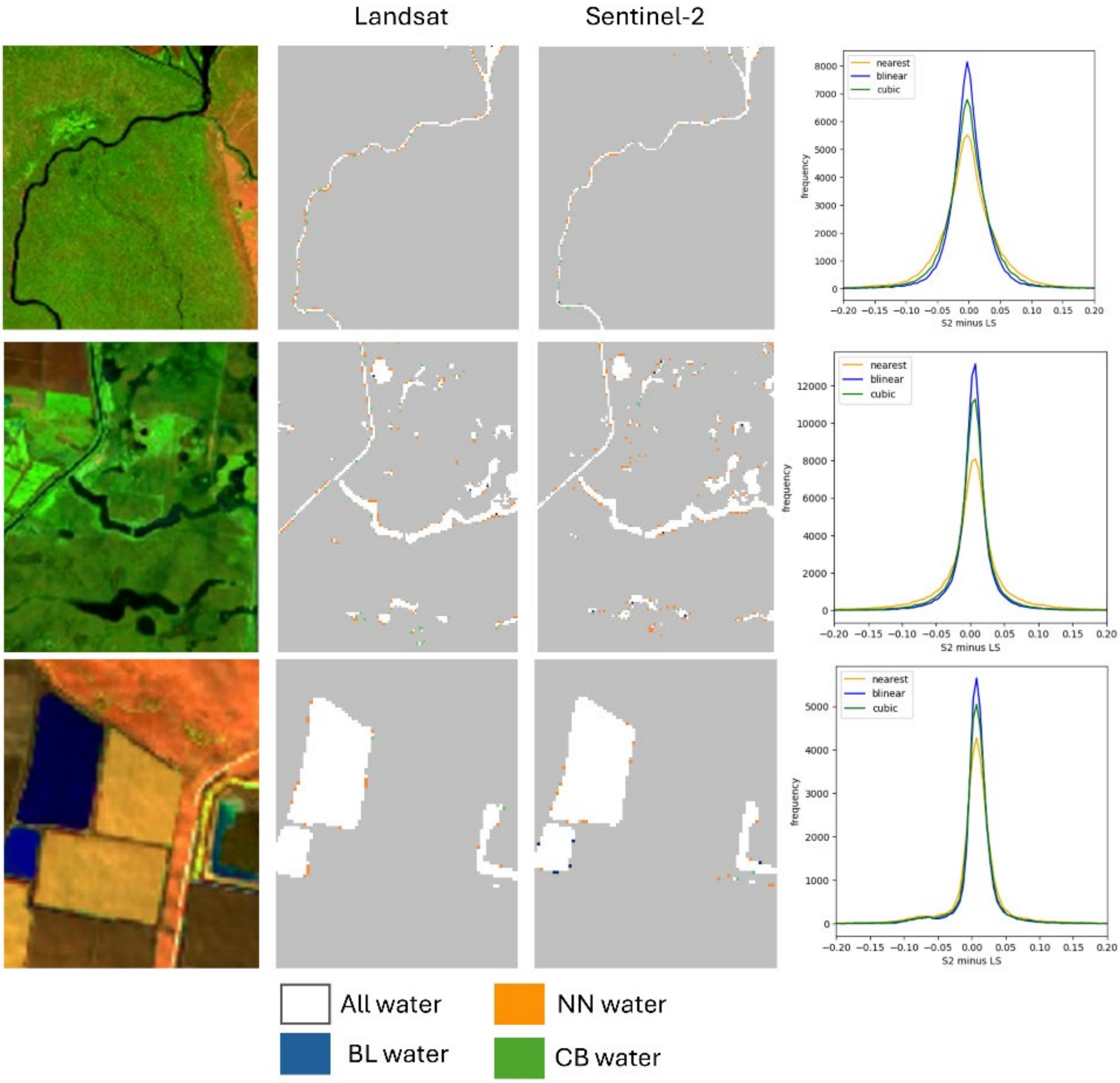

Figure 10 Influence of different resampling methods (nearest neighbour (NN), bilinear (BL), cubic convolution (CB)) between Sentinel-2 and Landsat imagery for detecting water.

2.3 Investigating new cloud masking algorithm

Cloud masking remains an issue when reading in Landsat data due to the difficulty in separating cloud shadow from water. It is also a major challenge when reading in the Sentinel-2 data (due to no Sentinel-2 thermal bands – which the Landsat fmask method utilises). A new cloud-masking layer (s2_cloudless_mask) is currently available through Digital Earth Australia, which works better than the Sentinel-2 fmask, although it does mask a lot of water bodies due to their similar appearance to cloud shadow. A new method has been tested to help remove the cloud and cloud shadow that is not automatically removed through Landsat's fmask and Sentinel-2's fmask for the monthly maximum MIM extent. For Sentinel-2 the s2cloudless_mask is also used to help identify cloudy scenes. This new method looks at the persistence of pixels that appear as bright cloud or dark shadow (and its classification in the fmask layer) throughout a month and removes images that are mostly cloud/shadow. Figure 11 (left) shows the maximum MIM water extent for September 2022 derived from Landsat and Sentinel-2 using its standard fmask and s2_cloudless_mask. Some areas are classified as water when they are obviously cloud. Figure 11 (right) shows the same maximum MIM water extent, but with the new cloud masking method applied. This method has removed all the cloud from the monthly composite in this example.

Figure 11 Maximum MIM water extent for September 2022 using standard fmask (left) and the new method (right).

2.4 Improving MIM method for wetlands

The wetlands layer used in the MIM method has also been updated. The MIM method relies on the Australian National Aquatic Ecosystem (ANAE) wetlands layer to determine which areas use the Tasseled Cap Wetness (TCW) index to map surface water in wetlands. The previous method only applied the TCW index to wetlands defined as lakes, bogs, swamps, etc, but not floodplains. This leads to differences between Victoria and NSW wetlands due to different definitions of these water bodies, leading to differences in water extent across the Victoria-NSW border. The new method now applies the TCW index to floodplain wetlands that are forested, as well as lakes, bogs, swamps, etc. This gives a more realistic classification of water in the forested wetlands such as the Barmah-Millewa forest. Figure 12 shows the old method (left) compared to the new method (right) for the percentage of observations from 1988 to 2021 when a pixel is wet.

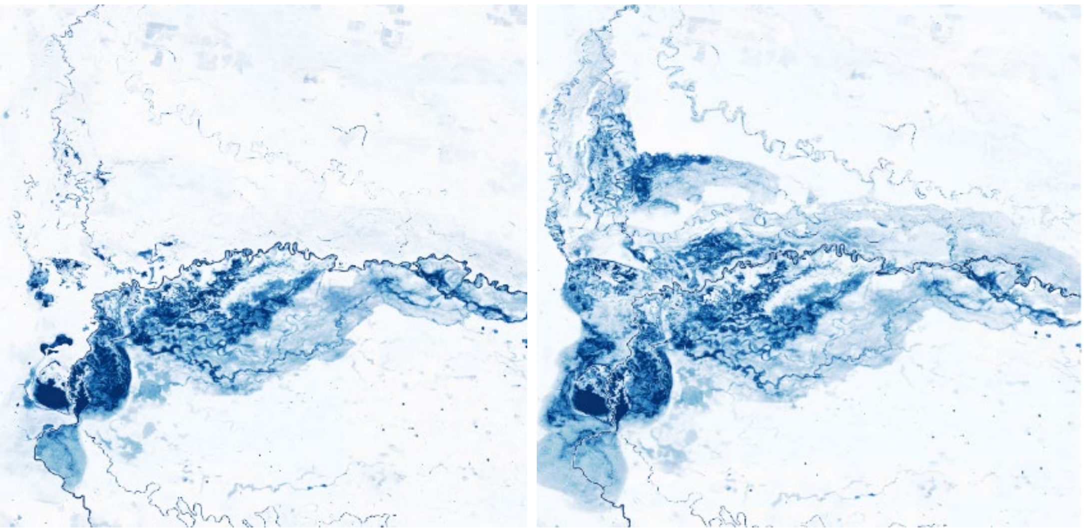

Figure 12 Comparison of the old method (left) and the new method (right) for improved classification of water in the forested wetlands in the Barmah-Millewa forest.

2.5 Developing an innovative method to detect water under vegetation

This section is adapted from Lymburner et al. (2024).

We have been working with Leo Lymburner (from Geoscience Australia who is spending a year at CSIRO) to improve the identification of water under vegetation. Current methods that use remote sensing to identify water under vegetation are challenging and underestimate water extent. We have developed a new method to map flooded forests (focusing on River Red Gum forests), which is based on the change to the Shortwave Infrared (SWIR) surface reflectance for surface water with forest cover. This has been written into a manuscript which has been published in Hydrological Processes: "Seeing the Floods through the Trees: Using Adaptive Shortwave Infrared thresholds to map Inundation under Wooded Wetlands" Leo Lymburner, Catherine Ticehurst, Maria Fernanda Adame, Ashmita Sengupta, Emad Khavei (Lymburner et al., 2024). A part of these findings (using a seasonal SWIR threshold to remove tree shadow) has been applied to the updated MIM.

Figure 13 below, which is Figure 10 from Lymburner et al. (2024), shows the water extent identified in the Gunbower, Pericoota, Koondrook site for 2016 and 2019, along with their flooded extent (in area) compared to nearby stream gauge stage height.

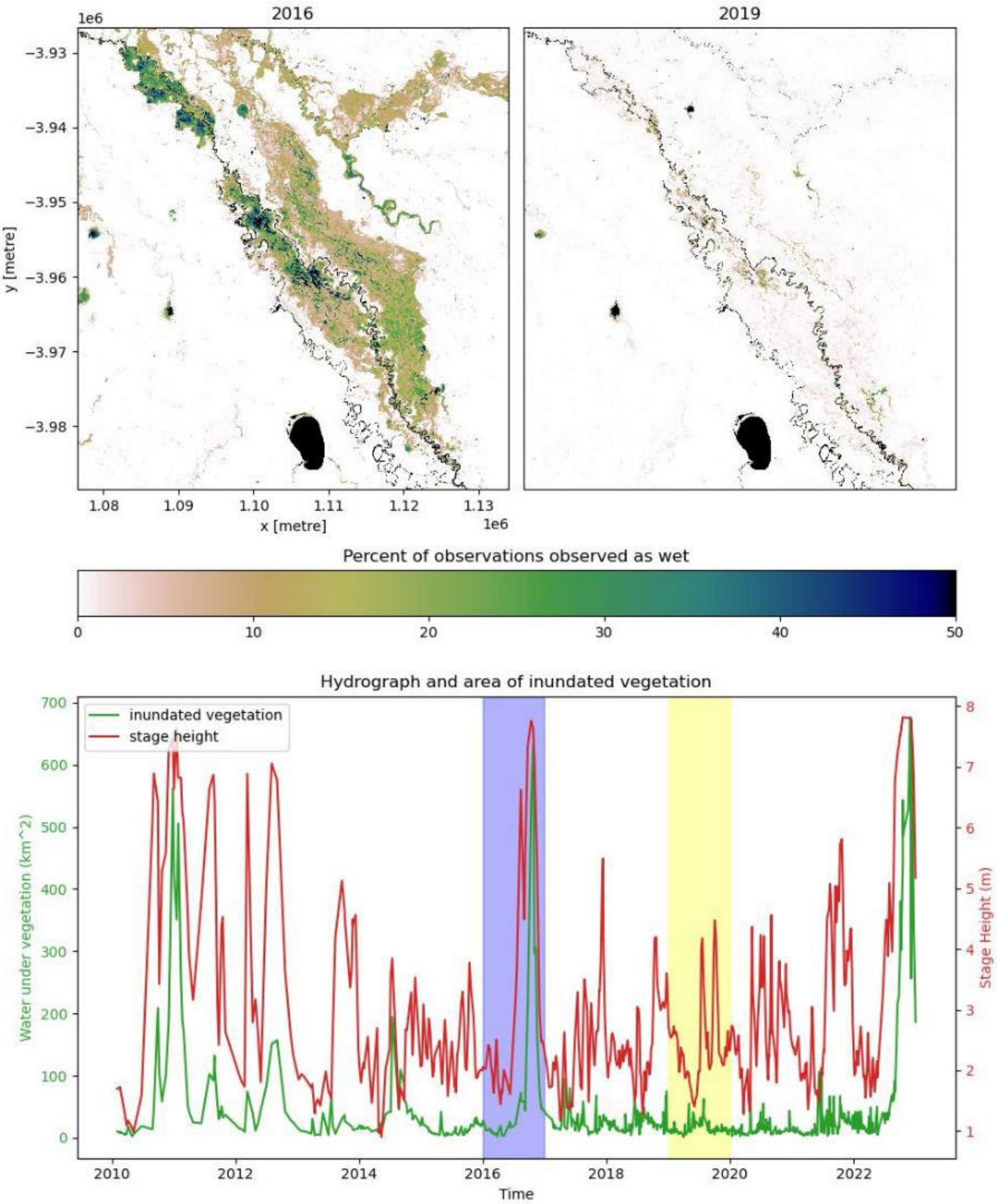

Figure 13 (Figure 10 from Lymburner et al. ,2024). Improved water extent identification in the Gunbower, Perricoota, Koondrook site for 2016 and 2019, along with their flooded extent (green) compared to nearby stream gauge stage height (red).

3 Benchmarking water depth estimation models

This section is adapted from Teng et al. (2022).

Simple models continue to be important for continental-scale floodwater depth mapping due to the prohibitively expensive cost of calibrating and applying hydrodynamic models. We have investigated the accuracy of three simple models for floodwater depth estimation from remote sensing derived water extent and/or Digital Elevation Models (DEMs) in semiarid regions. The three models are Height Above Nearest Drainage (HAND; Nobre et al., 2011), Teng Vaze Dutta (TVD; Teng et al., 2015b, 2019), and Floodwater Depth Estimation Tool (FwDET; Cohen et al., 2018).The model accuracy and nature of errors are established using industry's best practice hydrodynamic models as benchmarks in three regions in eastern Australia. The overall results show that FwDET tends to underestimate (by 0.32 m at 50th percentile) while HAND and TVD overestimate floodwater depth for almost all floods (by 0.97 and 0.98 m, respectively). We quantify how switching the DEM from 5 m LiDAR to national or global data sets DEM-H (Gallant et al., 2011), MERIT (Yamazaki et al., 2019), or FABDEM (Hawker et al., 2022) can affect different models differently; and we evaluate model performance against reach geomorphology and magnitude of flood events. The findings emphasize the importance of choosing a model that is fit for the intended application. By describing the applicability, advantages, and limitations of these models, this paper assists practitioners to choose the most appropriate model based on characteristics of their study area, type of problems they try to solve, and data availability.

As shown in Figure 14, HAND uses observed levels and a Digital Elevation Model (DEM) to calculate flood depth at address points. TVD uses an inundation extent raster and a slope-adjusted DEM to calculate the maximum surface water level across inundated areas. FwDET uses an inundation extent raster and a DEM to calculate depth by extrapolating between surface water levels identified along the perimeter of an inundation.

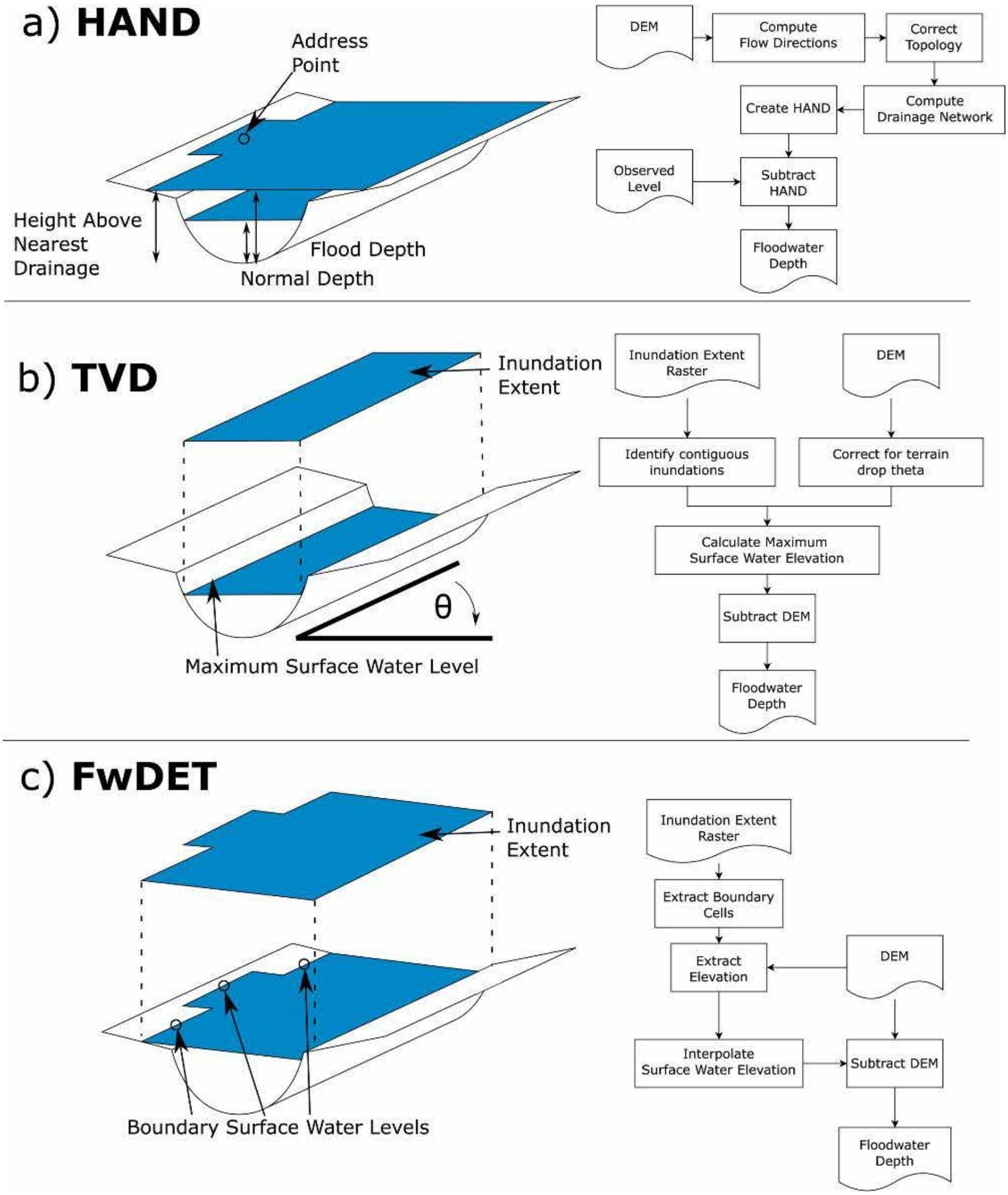

Figure 14 (Figure 2 from Teng et al., 2022). Conceptual models and processing steps for deriving depth from Height Above Nearest Drainage (HAND), Teng Vaze Dutta (TVD), and Floodwater Depth Estimation Tool (FwDET).

The differences between the water depth predictions from the three simple models and benchmark for the 26 flood scenes are shown in Figure 15. Positive values in Figure 15 represent underestimation of the water depth by the simple models and negative values represent overestimation. There is a large variation in the predictive capability of the three simple models, and there are also reasonable differences for each of the simple models for different flood/river reach combinations. Overall, HAND consistently overestimated the depths (substantial overestimation), TVD also consistently overestimated the depth (smaller overestimation compared to HAND), whereas FwDET consistently underestimated the water depths. There was no one model that consistently outperformed the others for all reaches.

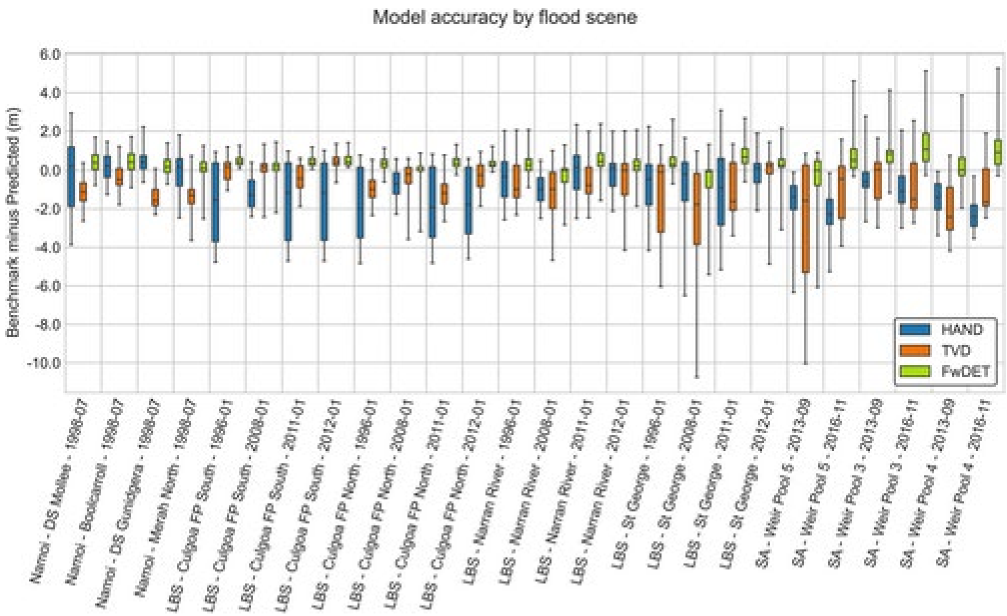

Figure 15 (Figure 3 from Teng et al., 2022). Difference between Height Above Nearest Drainage (blue), Teng Vaze Dutta (orange), and Floodwater Depth Estimation Tool (green) predictions and hydrodynamic model outputs (benchmark) for the 26 flood scenes. For each combination, the median is shown with a horizontal line, the boxes extend from 25th to 75th percentile and the whiskers from 2.5th to 97.5th percentile.

The overall results showed that FwDET had a tendency to underestimate floodwater depth (by 0.32 m at 50th percentile) while HAND and TVD overestimated floodwater depth for most floods (by 0.97 and 0.98 m, respectively).

FwDET was the most accurate at the floodplain edges with median MAE of 0.49 m for floodwater depths below 2 m, but the accuracy declined with deeper inundation (MAE of 1.41 m for water depth >4 m). All three models had similar performances for water depths between 2 and 4 m, but TVD provided better depth estimates for water depths above 4 m (MAE of 1.35 m). The distribution of FwDET errors for a combined analysis of 26 flood scenes was reasonably consistent and comparable with a Cauchy distribution, which suggests that similar errors could be expected for events/reaches outside our study area.

Model accuracy for all three models improved slightly with an increased magnitude of event, despite a weak correlation across validation data (R2 from 0.01 to 0.16). The evaluation of model performance against reach geomorphology showed that it is difficult to select a more suitable model based on the characteristics of the reach/floodplain. Although, as mean bank-full width increased, MAE increased for all three models (R2 of 0.19–0.46), which suggests it is generally more difficult to estimate depth in wider rivers (irrespective of the magnitude of flood being modelled).

For users who do not have access to a high resolution LiDAR DEM, a national or global DEM such as DEM-H, FABDEM, or MERIT could be used instead, expecting a decrease in model accuracy. This decrease is the least prominent with FwDET (median MAE increasing from 0.57 to 0.65–0.72 m in this study), followed by TVD and HAND. The results highlight that it is critical for HAND to use a hydrologically conditioned DEM to provide meaningful results.

The findings from this study showed that, while FwDET was the top performer overall, HAND was most suited for users with no/limited access to flood extents, and TVD performed the best for deep waters. This emphasizes the importance of using the appropriate model for the intended application, for example, spatial estimates of floodwater depth for emergency response such as road closures.

Given the various aspects of the modelling considered, the number of flood events examined, the number of hydrodynamic models used for validation, and the consistency with other literature, we expect that these findings would extend to other semiarid regions where similar input data are available.

4 Creating a Basin-wide water depth dataset

This section is adapted from Penton et al. (2023).

With growing concerns over water management in rivers worldwide, researchers are seeking innovative solutions to monitor and understand changing flood patterns. In a noteworthy advancement, stakeholders interested in the changing flood patterns of the Murray Darling Basin (MDB) in Australia, covering an area of 1 million km^2, can now access a consistent timeseries of water depth maps for the entire basin. The dataset covers the period from 1988 to 2022 at two-monthly timestep and was developed using remotely sensed imagery and a flood depth estimation model at a spatial resolution of ≈30 m, providing a comprehensive picture of maximum observed inundation depth across the MDB. Validation against 13 hydrodynamic model outputs for different parts of the MDB yielded a mean absolute error of 0.49 m, demonstrating reasonable accuracy and reliability of the dataset. The resulting dataset is best suited to system-wide analysis but might also be useful for those interested in the history of flooding at specific locations in the system. We provide the dataset, visualization tools, and examples to support ongoing research.

Figure 16 shows the workflow that generated flood depth products using the FwDET algorithm. The three panes show steps of the water depth product development. (a) Input data processing involves acquisition of two products: two-monthly maximum water surface extent (from Landsat) and a high-resolution Digital Elevation Model (combined from data sources), which we split into 23 regions for processing. (b) Floodwater Depth Estimation Tool (FwDET) algorithm v2 was used to identify the surface water elevation at the boundary (perimeter) of inundated areas. The perimeter water surface levels (elevations) were interpolated across inundated areas to provide continuous surface water levels. The depth was calculated by subtracting the Digital Elevation Model from the surface water levels and merging (recombining) across the Murray Darling Basin. (c) The resulting water depth rasters were archived in CSIRO’s Data Access Portal, and were also distributed through web services for machine access (i.e. Web Mapping Service) and presented through a geospatial visualisation platform for point-and-click visualisation of water depth across the floodplains of the Murray Darling Basin.

The two-monthly flood depth product provides a visualisation of specific events and a longitudinal perspective on flooding across the MDB. For users interested in specific events at a location, use the geospatial visualisation platform to confirm with local experts that the product has captured flooding in the areas expected to be inundated. The geospatial visualisation platform can be accessed through a web browser at https://map.csiro.easi-eo.solutions/. In the web browser, load the product by clicking ‘+Explore map data’, search the catalogue for ‘Flood Depth’ and click the ‘+’ next to the latest version of the flood depth product. The product will become visible once zoomed into a location of interest (inside the MDB). When satisfied, the maximum flood depth product for specific dates can be downloaded from CSIRO’s Data Access Portal (DAP) for ingestion into a GIS application. If confirming with local experts is not practicable, alternatives include searching archives such as Geoscience Australia’s Australian Flood Risk Information Portal, aerial photography archives – e.g. New South Wales Historical Satellite Imagery, media reports or social media.

For researchers interested in the longitudinal perspective on flooding across the MDB, it is necessary to access the whole dataset from CSIRO's DAP. A Python Jupyter Notebook (example_water_depth.ipynb) provided as part of the code gives an example of selecting time periods (2021–2022), spatially sub-setting the data (e.g. near Macquarie Marshes Nature Reserve), visualising recent events and undertaking rudimentary statistical analysis. The notebook provides an example of calculating a short timeseries of water volumes and incorporating bias-correction.

The study's findings have substantial broader impacts, benefiting communities, flood managers, decisionmakers, environmental conservation, and stakeholders in the MDB. The dataset supports evidence-based decision-making and ongoing research.

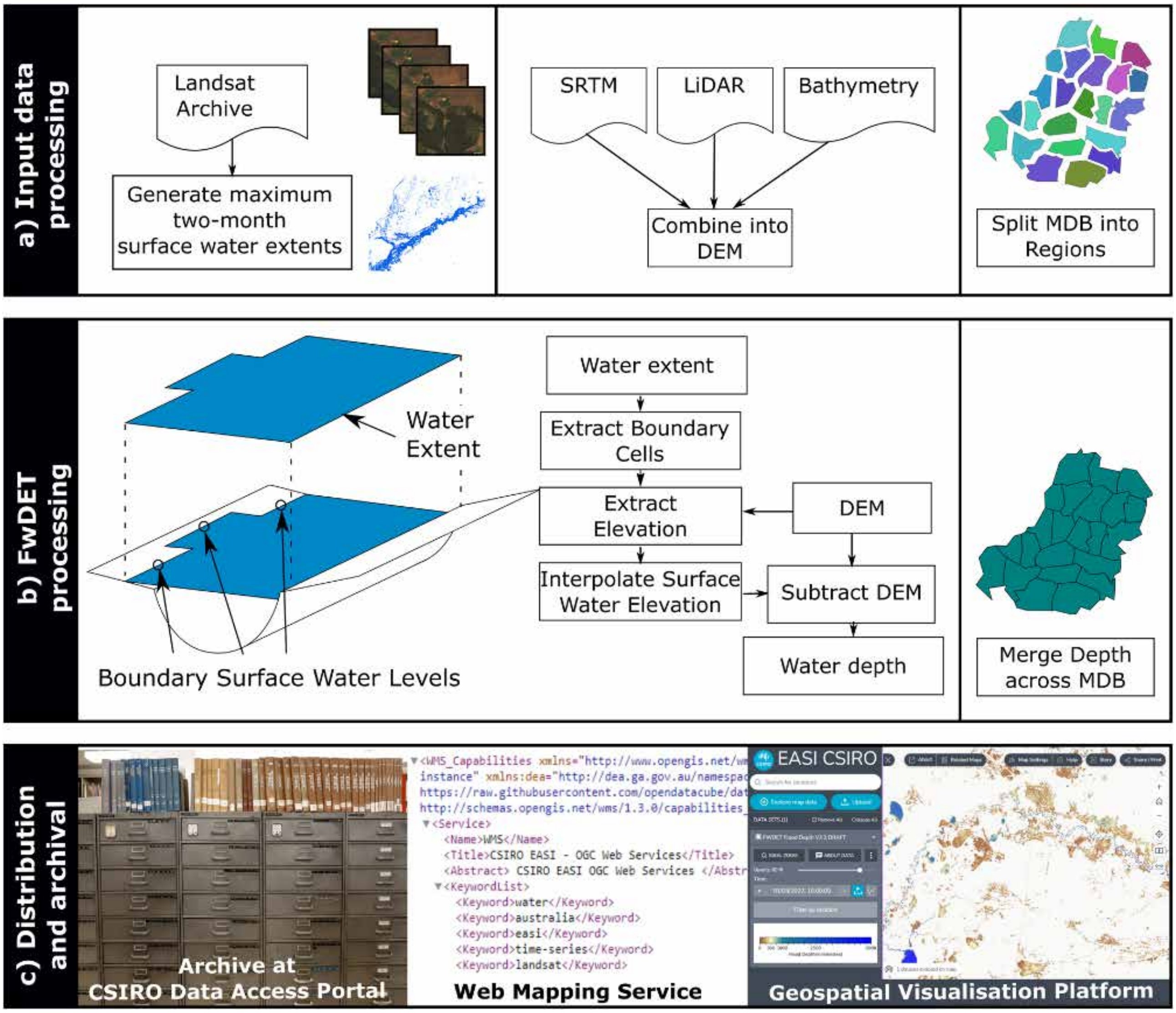

Figure 16 (Fig 2 from Penton et al., 2023) Steps involved in building and distributing the flood water depth product for the Murray Darling Basin.

5 Development of a floodplain ecological response model

This section is adapted from Teng et al. (2024a).

Quantitative assessment of floodplain ecological response to flow regimes is challenging but essential for setting targets and estimating impacts for environmental water management. We have developed a model, as described in Figure 17, which takes long-term (90 years) and large-scale (9 million grid cells) flood maps as input to estimate the response of floodplain vegetation using infinitely differentiable functions. The model, named Floodplain Ecological Response Model (FERM), is calibrated against 1-D temporal Leaf Area Index (LAI) data from the WAVES energy and water balance model at a daily timestep, and validated on the entire floodplain using condition data of the Icon Sites of the Murray River aggregated to a yearly timestep. Results show that FERM can adequately simulate the response of different types of vegetation on the floodplain, while reducing the data requirements and runtime drastically compared to other approaches. The FERM modelling approach is a first step towards a quantitative modelling of floodplain forest ecosystems at large scale with realistic data and computation requirements. It is intended to indicate the potential of such an approach in semi-arid systems where data availability is limited, and to encourage the further research needed to improve our understanding of floodplain forests and our capacity to model the impact of floods on their ecological response.

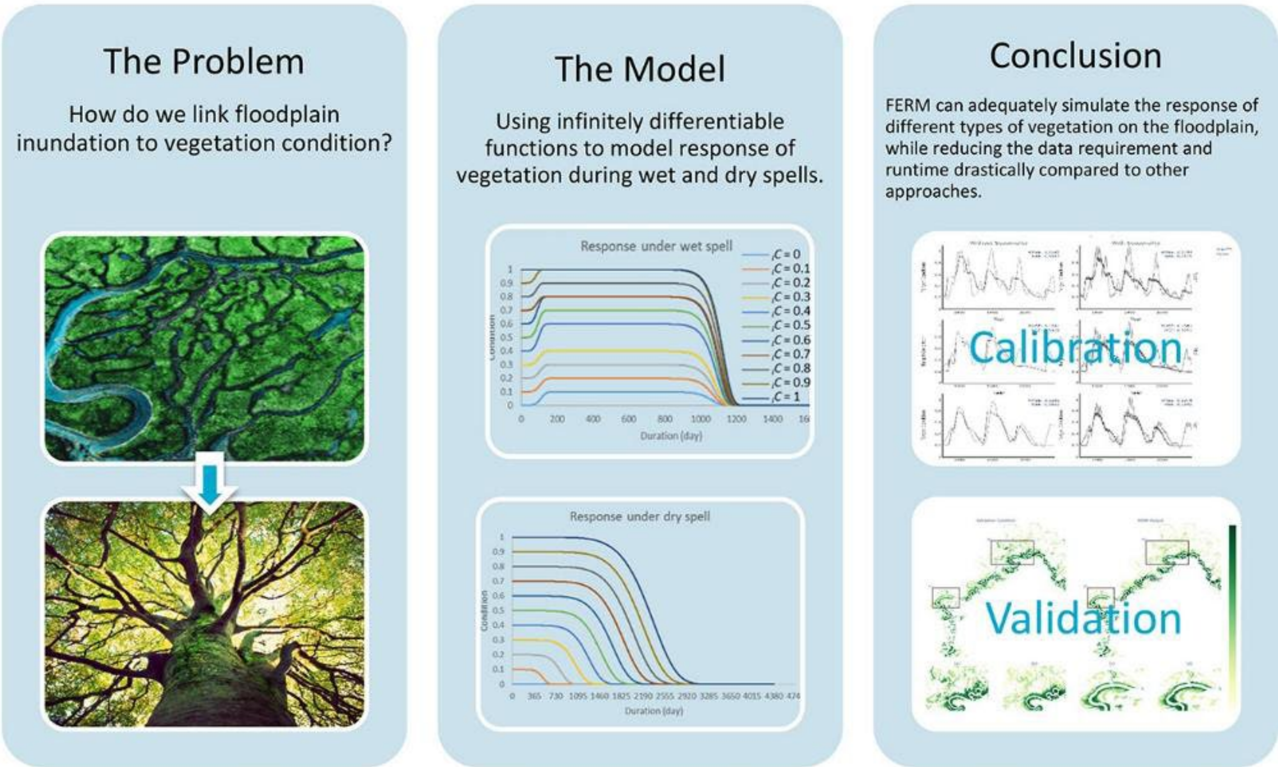

Figure 17 Graphic abstract of Teng et al. (2024a.)

6 Linking floodplain inundation with climate

This section is adapted from Teng et al. (2024b).

The two-monthly maximum water depth maps of Teng et al. (2023) provide a comprehensive quantitative description of floodplain inundation over the past 35 years (1988–2022). We quantified inundation frequency or average recurrence interval (ARI) and trends over the past 35 years, which provided important information about basin wide connectivity, ecological hotspots, and potential habitats for restoration (Teng et al., 2024). In the MDB, the flood-affected area (i.e., with ARI≤ 35 years) covered approximately 274,049 km^2, representing 25.9% of the total MDB area. The region with high flood inundation frequency (i.e., ARI≤ 2 years) encompassed around 30,400 km^2, with a mean elevation of 147.5 m. Meanwhile, the area with medium flood inundation frequency (ARI between 8-16 years) spanned approximately 79,204 km^2, with a mean elevation of 152.3 m.

We found that the proportion of flood-affected areas of Northern MDB (24.8%) was lower than Southern MDB (27.1%), while the area proportion of high inundation risk was higher in Northern MDB (3.0%) compared to Southern MDB (2.8%). Results indicate that Northern MDB may experience lower flooding risks than Southern MDB but could be more severely affected by extreme inundation events.

Flood inundation is largely determined by hydroclimate conditions. Identifying the dominant hydroclimate drivers can contribute to predicting flood inundation potentials under a changing climate. Figure 18 shows the correlation of the rainfall and runoff metrics against the annual maximum flooding water extent.

We found that most of the hydroclimate variables considered were generally correlated well with the annual maximum flooding water volume and hence inundation extent. The maximum 30-day streamflow was overall the most dominant driver of flood inundation and a suitable proxy for predicting flood extent and volume under a changing climate.

Correlations between flood inundation and dominant hydroclimate variables were found to be stronger in the Northern Basin than the Southern Basin, indicating that the Northern Basin is more responsive to hydroclimate change in terms of flood inundation.

.

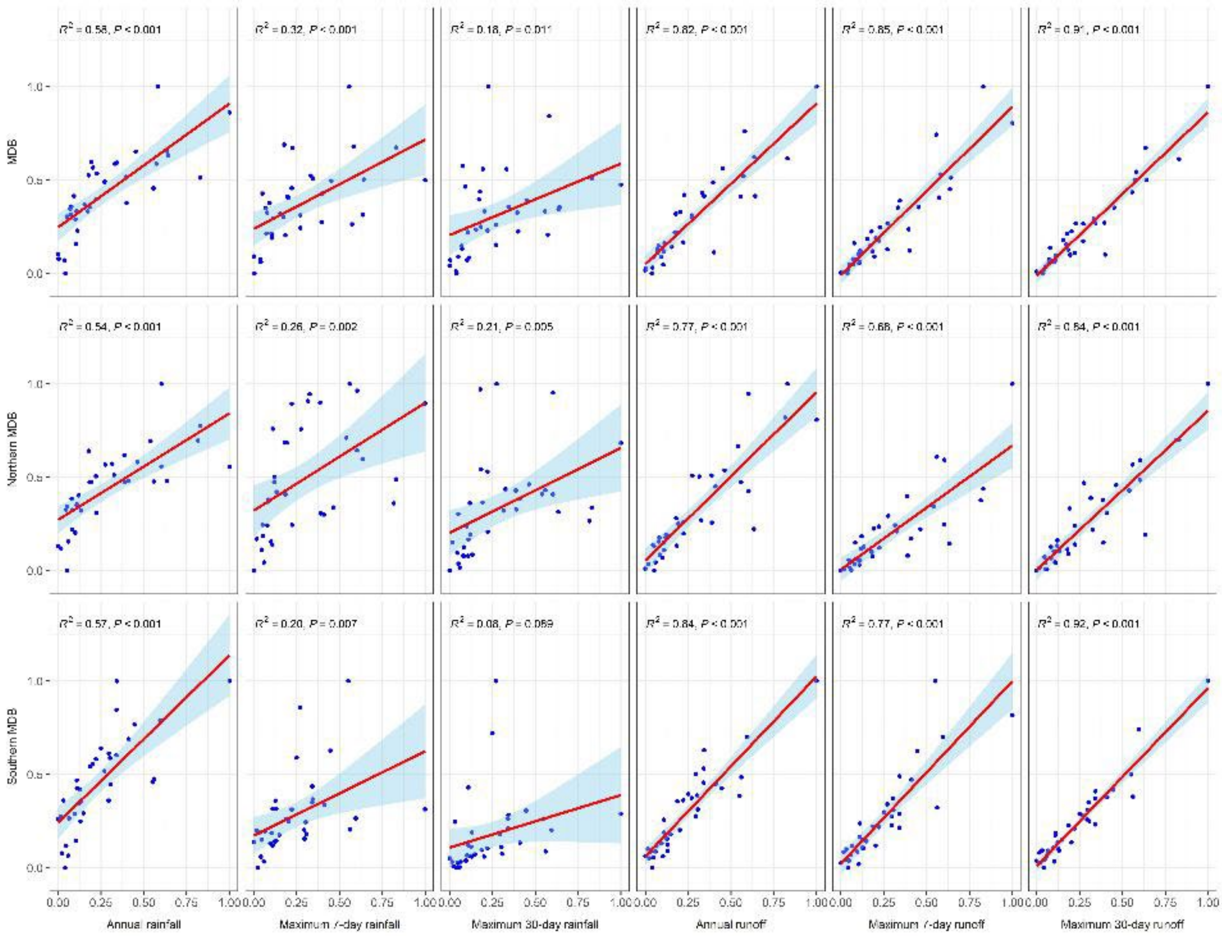

Figure 18 (Figure 3 from Teng et al., 2024b) Relations between maximum inundation extent and hydroclimatic variables. x-axis is scaled hydroclimatic variables, y-axis is scaled maximum inundation extent.

We characterised the 35-year perspective of inundation frequency in comparison to the instrumental historical 123-year period (1900-2022) and future projections under climate change informed by CMIP6 GCMs. The analyses showed that the Annual Exceedance Probabilities (AEPs) of modelled runoff in the 35-year period were higher than those of the 123-year period. Especially for the large flood events (see Figure 19).

While future climate projections indicate a drier MDB with lower mean annual runoff, the projections for changes in future floodplain inundation are less significant, as illustrated by Figure 19. This is due to the compensating effects of more intense extreme high rainfall versus drier antecedent catchment conditions under climate change. For the Southern MDB, projected AEP of the inundation proxy is mostly close to that of the century-long baseline. In the Northern MDB, however, moderate to severe floods (AEP < 0.05) are projected to increase, while more frequent floods are expected to stay within historical bonds.

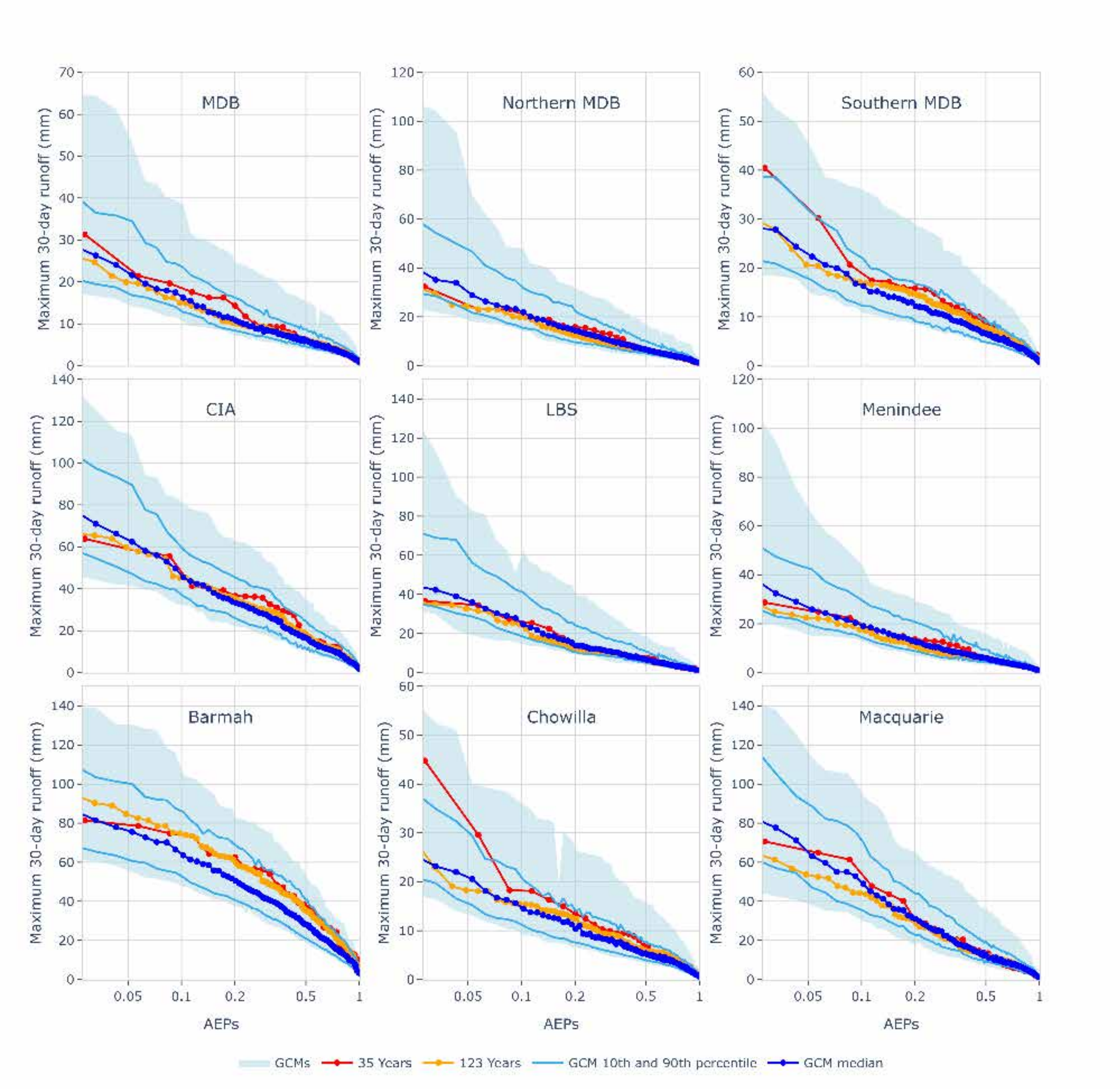

Figure 19 (Figure 4 from Teng et al., 2024b) Comparison of recent, historical, and future floodplain inundation annual exceedance probabilities. AEPs for the recent observational 35 years, historical 123 years, and future projections, where an AEP of 0.05 is equivalent to 1-in-20 year floodplain inundation, and similarly 0.1 – 1-in-10 year, 0.2 – 1-in-5 year, 0.5 – 1-in-2 year, 1 – 1-in-1 year. The modelled future projections are shown as light blue shades with the median shown as dark blue lines.

The knowledge from this study has significant implications for communities, decision-makers, environmental watering efforts, and stakeholders within the MDB. We found that the maximum 30-day runoff closely correlates with flood inundation in the MDB. This finding offers a reliable proxy for flood inundation, which is critical given the challenges in obtaining spatial inundation data. It also implies that, even with anthropological influences, the natural hydrological processes continue to play a dominant role in flood dynamics within the basin. Understanding this correlation can aid in better predicting and mitigating the impacts of flooding.

Part III Datasets

1 Introduction

In addition to the input datasets discussed in Part I, several basin-wide datasets have been developed to support researchers and stakeholders in understanding the evolving flood patterns within the MDB. These datasets include consistent time series of water depth maps covering the entire basin, a feat that was historically challenging to achieve on a large scale. Spanning from 1988 to 2024, with data points every one to two months, these datasets were generated using remotely sensed imagery and flood perimeter models at an approximate spatial resolution of 30 meters. This comprehensive collection provides a detailed depiction of maximum observed inundation depths across the MDB, making it ideal for system-wide analyses as well as for investigating the flooding history at specific locations within the basin.

The development of these datasets leveraged the knowledge and input datasets acquired through the research activities conducted throughout the RQ7 project (see Part II). Utilizing state-of-the-art models, the datasets were meticulously validated against observational data and hydrodynamic models to ensure their accuracy and reliability. To facilitate ongoing research, we are providing not only the datasets but also visualization tools and illustrative examples.

These datasets are instrumental in examining the relationship between flooding and ecological functions, particularly suited for long-term analyses of the MDB as a whole. For example, researchers can utilize the data to explore the physical and biological connectivity of floodplains and track how these connections have evolved over time. Additionally, the datasets are ideal for developing empirical relationships between flooding events and ecosystem processes. While they are highly beneficial for analysing the flood history of specific areas within the river system, it is recommended to verify their accuracy with local data sources where necessary.

Figure 20 illustrates an example of the maximum floodwater depth computed over a 35-year period. Notably, linear features running approximately north-south are visible in the image, which are attributed to noise from the swath edges of Landsat 5 images during its later operational years. These artifacts result from pixels being incorrectly classified as water, highlighting the importance of careful data interpretation.

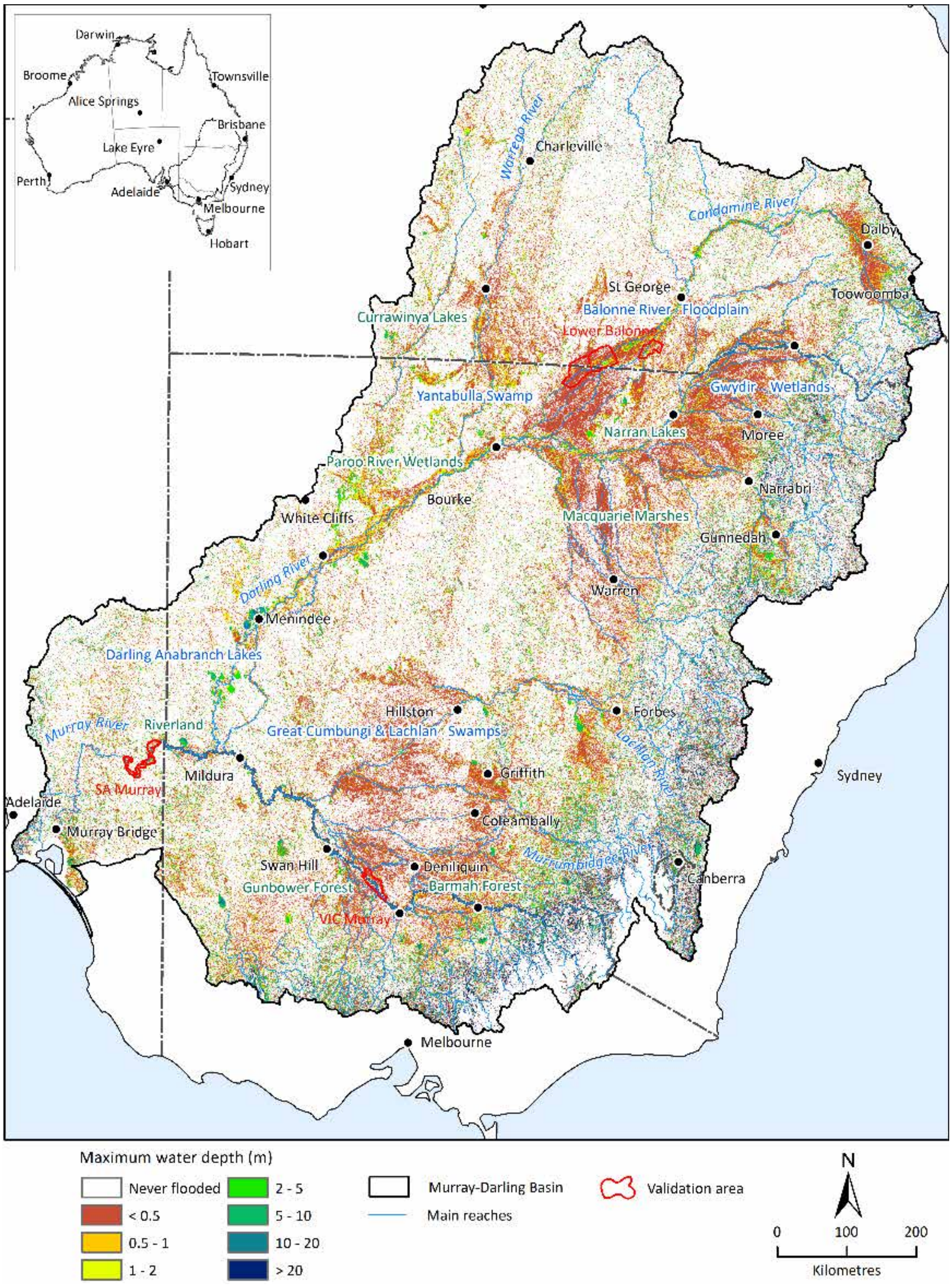

Figure 20 (Figure 1 from Penton et al., 2023) Maximum floodwater depth. The maximum floodwater depth for MDB calculated from the two-monthly floodwater depth dataset.

2 List of datasets and brief descriptions

Table 7 Datasets on CSIRO Data Access Portal (DAP).

Name	DOI	Brief Description
LIDAR enhanced SRTM Digital Elevation Model (DEM) for Murray Darling Basin	https://doi.org/10.25919/5n0m-1682	Digital Elevation Models (DEMs) for the Murray-Darling Basin at 1 arc second, 25 metre and 5 metre resolution. Elevation for the whole MDB sourced from LIDAR where available in June 2021 and backfilled with hydrologically enforced 1 second SRTM. Developed as part of the Murray-Darling Water and Environment Research Program and Murray-Darling Ecosystems Function Project.
Hydrodynamic modelling results collection	https://data.csiro.au/collection/csiro:54823	Hydrodynamic model calibration results were collected from previous flood modelling projects carried out in MDB by SA Department for Environment and Water (DEW), CSIRO, MDBA and NSW Office of Environment and Heritage (now NSW Department of Planning and Environment or DPE) for the development and validation of a predictive flood inundation and volume model. This collection has been released to a specified group of authorised users for their use only.
Gauged Data for the Murray-Darling Basin	https://data.csiro.au/collection/csiro:54834	This data collection is for the gauged data that was used in the project. There are two main types of gauge data in this collection: 1) gauge network information, and 2) time series at the gauges. The information for each gauge were gathered from five sources: Bureau of Meteorology (BoM) for the streamflow data, and other information from the South Australian government, Queensland government, MDBA and the Australian Water Resources Assessment – River (AWRA-R) modelling team. This collection has been released

		to a specified group of authorised users for their use only.
Maximum two-monthly surface water extent for MDB from MIM and WOFS	https://doi.org/10.25919/wkg9-7t35	The multi-index method (MIM) (refer to Ticehurst, Teng and Sengupta 2022 in the Related Links for a description of the method) was developed for mapping surface water across the Murray-Darling Basin (MDB) based on Landsat surface reflectance data available in Digital Earth Australia. More than thirty years of two-monthly images of surface water extent across the whole MDB have been produced using this method, along with Water Observations from Space (WOfS) to fill in any gaps associated with cloud cover due to the different cloud masks used. The data were produced as part of the Murray-Darling Basin Ecosystem Function (MDB-EF) and Murray-Darling Water and Environment Research Program (MD-WERP) projects. Note that a new improved version has been developed and is expected to be released late 2022.
Two-monthly Maximum Flood Water Depth Spatial Timeseries for the MDB	https://doi.org/10.25919/c5ab-h019	The two-monthly spatial layers of flooding was developed to represent maximum surface water extent and water depth within each two-month period across the Murray-Darling Basin (MDB). This work is based on the multi-index method (MIM) surface water mapping and Digital Elevation Model (DEM) using the Floodwater Depth Estimation Tool (FwDET). More than thirty years of two-monthly images of surface water depth across the whole MDB have been produced using an improved version of the Floodwater Depth Estimation Tool (FwDET), first developed by Cohen et al. (2018). The flood water depth was estimated based on spatial time series of two-monthly maximum multi-index surface water extents

Data for assessing floodwater depth estimation models HAND, TVD and FwDET	https://doi.org/10.25919/sq5q-6070	Data resulting from comparison of Height Above Nearest Drainage (HAND; Nobre et al., 2011), Teng Vaze Dutta (TVD; Teng et al., 2013) and Floodwater Depth Estimation Tool (FwDET; Cohen et al., 2018) with hydrodynamic models to produce figures and graphs.
Maximum two-monthly surface water extent for MDB from MIM and WOFS - Version 2	https://doi.org/10.25919/es0k-q169	The multi-index method (MIM) (refer to Ticehurst, Teng and Sengupta 2022 in the Related Links for a description of the method) was developed for mapping surface water across the Murray-Darling Basin (MDB) based on Landsat surface reflectance data available in Digital Earth Australia. More than thirty years of two-monthly images of surface water extent across the whole MDB have been produced using this method, along with Water Observations from Space (WOfS) to help fill in gaps associated with cloud cover. This is Version 2 of this product, spanning from 1988 to June 2022, with an updated version from 1988 to December 2022.
Persistent water within the MDB from MIM	https://doi.org/10.25919/x1d1-pz44	Thirty-three years of minimum monthly images of surface water extent have been used to identify persistent water within the Murray-Darling Basin (MDB). The multi-index method (MIM) (refer to Ticehurst, Teng and Sengupta 2022 in the Related Links for a description of the method) was used for mapping surface water across the MDB based on Landsat surface reflectance data available in Digital Earth Australia. Persistent water layers are provided for 1988 to 2020, 1990 to 1999, 2000 to 2009 and 2010 to 2019.
Maximum number of consecutive dry years from two-monthly surface water extent for MDB	https://doi.org/10.25919/8tvg-d885	The multi-index method (MIM) (refer to Ticehurst, Teng and Sengupta 2022 in the Related Links for a description of the method) was developed for mapping surface water across the Murray-Darling Basin (MDB) based on Landsat surface reflectance data

using MIM and WOFS		available in Digital Earth Australia. More than thirty years of two-monthly images of surface water extent across the whole MDB have been produced using this method, along with Water Observations from Space (WOfS) to fill in any gaps associated with cloud cover due to the different cloud masks used. The maximum annual water extent was derived from the MIM-WOfS layers, which were then used to calculate the maximum number of consecutive years that a pixel is dry from 1988 to 2022, and 2010 to 2022 (which excludes the Millenium Drought).
EASI OWS web service	https://data.csiro.au/collection/csiro:57955	Earth Analytics Science Innovation (EASI) platform OWS web services (WMC, WCS etc), used to publish large scale spatial data. Visualisation tools and simple analysis tools were provided via web browsers.
Bathymetry-embedded DEM for the Murray-Darling Basin version 2	https://doi.org/10.25919/t0rw-4e80	Basin-wide Digital Elevation Models (DEMs) with embedded bathymetry for selected main rivers Murray-Darling Basin at 5 metre (GDA2020 Lambert Conformal Conic) and 1 second (WGS 1984) resolution. Elevation for the whole MDB sourced from lidar and photogrammetry where available, from the Geoscience Australia elevation data platform in November 2022, and backfilled with the Forests and Buildings Removed global DEM (FABDEM). Developed as part of the Seamless merging of DEMs project in the CSIRO Environment Digital Water and Landscapes initiative. Where available, channel bathymetry data were then merged with the MDB DEM at 5 m resolution.
Maximum two-monthly surface water extent for MDB	https://doi.org/10.25919/zjec-k149	Updated version from V2 with the following improvements: • Using a new cloud-masking method.

from MIM - Version 2024		• Refined water detection from Landsat imagery in wetlands and vegetated areas. • Updated to June 2024.
Maximum monthly surface water extent for MDB from MIM using Landsat and Sentinel-2	https://doi.org/10.25919/z1nc-md19	Similar to above but transitions from two-monthly to monthly frequency with integration of Sentinel-2 data from 2016 onwards.
Two-monthly Maximum Flood Water Depth Spatial Timeseries for the MDB Version 2024	https://data.csiro.au/collection/csiro:64061	Two-monthly water depth dataset based on water extent Version 2024 with water depth estimation through the use of a bathymetry-enforced DEM.
Monthly Maximum Flood Water Depth Spatial Timeseries for the MDB	https://data.csiro.au/collection/csiro:64062	Monthly water depth dataset based on monthly water extent with water depth estimation using water depth estimation through the use of a bathymetry-enforced DEM

Part IV RQ7 Model

This part is adapted from Teng et al. (2025).

1 Introduction

As the main focus of the RQ7 project, we have developed a daily flood inundation model (the RQ7 model) that combined the strengths of an empirical model (RiM-FIM) and a simple conceptual model (TVD). The RQ7 model was designed for application across major floodplain reaches in the MDB to predict flood inundation extent, depth, and duration by integrating Landsat-derived water extents, high-resolution DEMs, and river flow measurements.

To achieve this, we utilized MIM water extents derived from Landsat and Sentinel-2 imagery of historical flood events. Water depth was estimated using FwDET based on the latest basin-wide DEM. We built a relationship between gauged flow characteristics and inundation volume using random forest regression. In areas lacking observations, we interpolated based on elevation, adopting a methodology similar to RiM-FIM but using the TVD approach to reduce depths from higher water levels and eliminate disconnected floodplain areas. A volume-tracking component was also developed to estimate daily volume gains and losses on the floodplain, ensuring the closure of the water balance.

The model was developed on the Earth Analytics Science and Innovation (EASI) platform, a high-performance data analytics platform that integrates extensive Earth Observation (EO) data with other geospatial information and models. The RQ7 model was created using Jupyter notebooks on EASI JupyterHub (https://hub.csiro.easi-eo.solutions/hub/spawn) and utilized cloud computing via Amazon Web Services (AWS) Elastic Compute Cloud (EC2). The model code was managed on GitHub (https://github.com/MDBAuth/RQ7), leveraging the distributed version control of Git. Input and output data were stored on Amazon Simple Storage Service (Amazon S3), accessible through the EASI platform or the AWS management console (https://csiro.awsapps.com/start#/), enabling modellers to access the data from anywhere with a web browser.

We used the Open Data Cube for spatiotemporal analysis, multi-index methods for water detection, and both Landsat and Sentinel-2 imagery. Additionally, we explored the potential for integrating emerging technologies as they became available. The model underwent rigorous testing and validation against available observations and hydrodynamic model outputs at five key locations in the MDB, ensuring its reliability and accuracy.

The RQ7 model enabled more accurate and comprehensive flood inundation predictions, supporting systematic management and scenario planning across large areas and long simulation periods in the MDB.

2 Model structure

The RQ7 model consists of four key components and a series of tools, visually represented in Figure 21. Below is a description of these key components:

2.1.1 Library builder

This component constructs a library of water depth images.

Inputs:

i. Boundary of study window and exclusive areas
ii. Floodplain footprint mask
iii. Gauged streamflow timeseries
iv. DEM and spatial masks, e.g. cloud mask, cover masks, etc.
v. Landsat and Sentinel 2 images accessed via Open Data Cube

Outputs:

i. Library of flood extent and water depth images
ii. A table summarises the statistics of the library: date, flood volume, streamflow characteristics (streamflow on the day, mean streamflow of previous 3,5,7,10,15,20,25,30,90 days)

Modules:

i. 1_library_generation.ipynb

2.1.2 Flood volume predictor

This component builds a model/relationship linking streamflow metrics with the flood extent and water depth library using a machine learning technique – random forest regression.

Inputs:

i. Daily streamflow timeseries (hydrograph)
ii. The library summary csv file from the first component

Outputs:

i. Predicted flood volumes
ii. Performance summary

Modules:

i. 2_flood_volume_prediction.ipynb

2.1.3 Water depth image generator

This component creates water depth images for each day of the input hydrograph through interpolation of two images from the library.

Inputs:

i. The predicted flood volume from the second component and image library from the first component

Outputs:

i. The predicted water depth image for each day of the input hydrograph

Modules:

i. 3_Geotiff_generation.ipynb

2.1.4 Floodplain volume tracker

This component generates volume gain and loss for each day of the input hydrograph.

Inputs:

i. The predicted water depth image for each date of the input hydrograph
ii. SILO rainfall and ET via Open Data Cube
iii. Soil property layers derived from the nation-wide AWRA soils data

Outputs:

i. The predicted volume gain and volume loss for each date of the input hydrograph
ii. Soil moisture content for each day

Modules:

i. 4_volume_tracker.ipynb

2.1.5 Tools

i. check_flow_volume.ipynb: creates floodplain volume statistics to identify problematic input images.
ii. get_streamflow_from_bom.ipynb: downloads and formats the streamflow data from BoM's Water Data Online website.
iii. RQ7_runner.ipynb: runs the model components in sequence.
iv. spatial_correlations.ipynb: calculates spearman's correlations to identify potential exclusion areas.

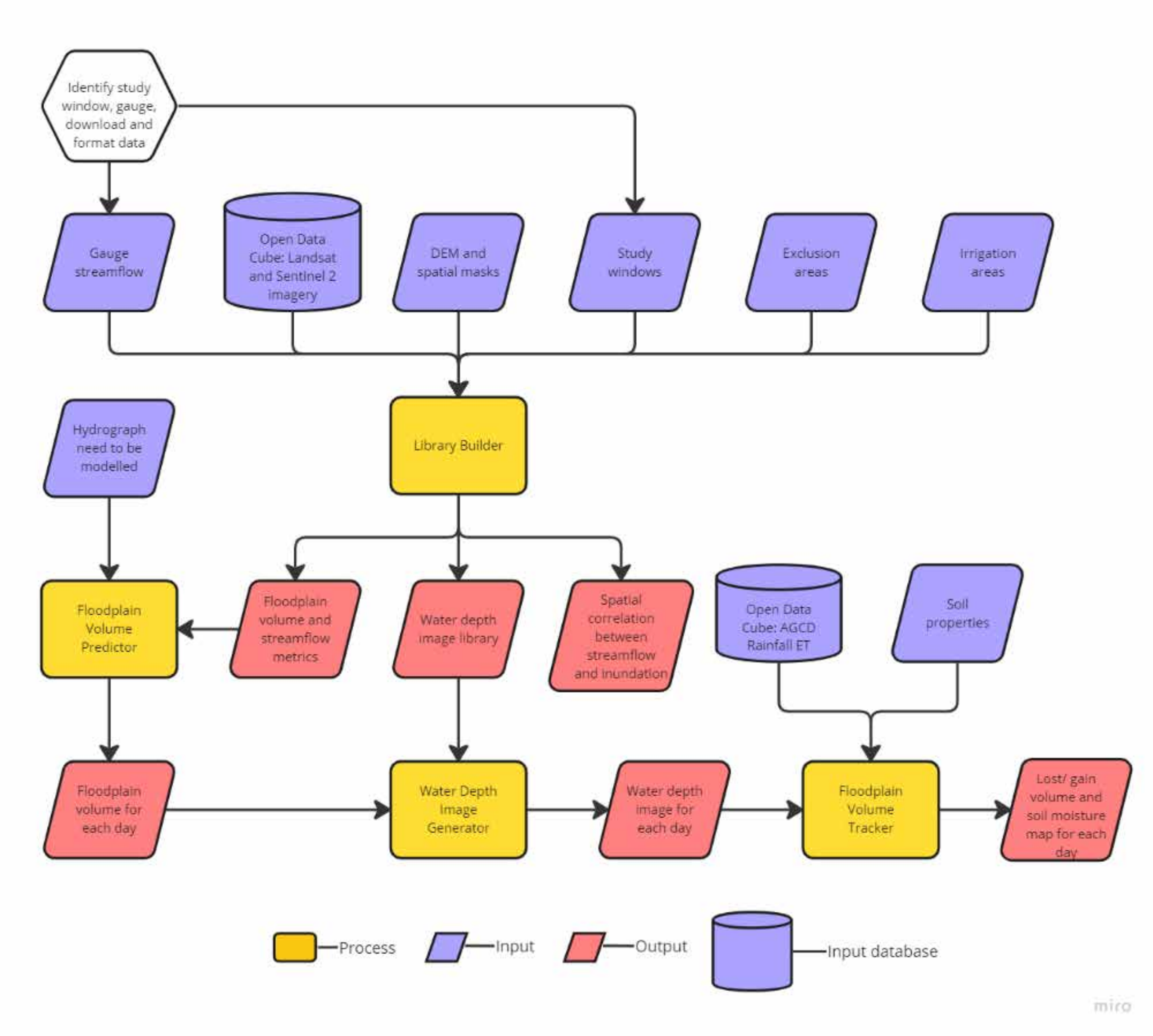

Figure 21 Flow chart showing the structure of the RQ7 model.

3 Model validation

The RQ7 model underwent rigorous testing at five key locations, encompassing a total of seven reaches: the Lower Balonne System (LBS_422204), South Australia Murray (SA_A4260515), Namoi (Namoi_419039), Gunbower (Gunbower_409207), and three reaches in the Lower Murrumbidgee (WP6_410036, WP10_410136, WP12_410041). Initial results have been promising, demonstrating strong agreement between the modelled and observed water extents. Ongoing updates to the model code are incorporating the latest advancements outlined in Part II, further enhancing its accuracy and utility.

The validation process for the RQ7 model's flood water extent and depth predictions involved three key steps:

1. Comparison with Satellite-Derived Water Extents:
   The model was run over a historical period that included dates for which satellite imagery was available. The modelled water extent was compared to the Multi-Index Method (MIM)-derived water extent for those dates, and F-statistics (F-stat) were calculated to measure the accuracy of the flood extent predictions. The F-statistics, defined as $\frac{A_{op}}{A_{o+}A_{p}-A_{op}}$ where A_o is the observed inundation area (from the benchmark), A_p is the modelled inundation area, and A_{op} is the overlapping area, provide a quantitative measure of model performance (Dey et al., 2019).

2. Comparison with Hydrodynamic Models:
   The model was also run for periods corresponding to the calibration times of hydrodynamic models. The resulting water extent and water depth predictions from the RQ7 model were compared against outputs from the hydrodynamic models to evaluate alignment.

3. Validation Against Remote Sensing and Aerial Photos:
   Finally, the flood water extent predicted by both the RQ7 model and the hydrodynamic models was compared to water extent data derived from remote sensing images or aerial photographs taken during the calibration periods of the hydrodynamic models.

These validation steps not only highlight the RQ7 model's capability to simulate large-scale flood events over extended periods but also provide a robust framework for assessing its strengths and identifying areas for improvement. The outcomes offer an invaluable resource for researchers and stakeholders, enabling them to better understand the model's potential and limitations and apply it effectively to manage the complex hydrological and ecological dynamics of floodplains in the MDB.

3.1 Initial testing sites and planning for model upscaling

The initial testing sites were chosen to reflect the diversity of riverine environments found in the MDB while aligning with the best available models and datasets. The available hydrodynamic modelling datasets described in Section 4.2 were used as benchmark to validate the model results. The initial testing sites encompass five locations, and seven river reaches in the MDB (Figure 8 and Figure 22). In total, seven calibration events were used in the validation of the model (Table 3).

We have also developed methods to expand the model to other parts of the MDB. This requires the division of the Basin into appropriately sized regions through which water can travel in around one day (to be consistent with the daily time step of the river system model). We have investigated Thiessen polygon and residual catchment for the Australian Water Resource Assessment – River System Model (AWRA-R) gauges. The 3D lengths for main channels within each region were also calculated. We have collected data that are required to estimate average velocity, along with the 3D length, so the appropriate size of each region can be determined. Some gauges were eliminated, and some dummy gauges were included so that the density of the gauges is even across the Basin. The resulting 247 modelling windows across the MDB are shown in Figure 22.

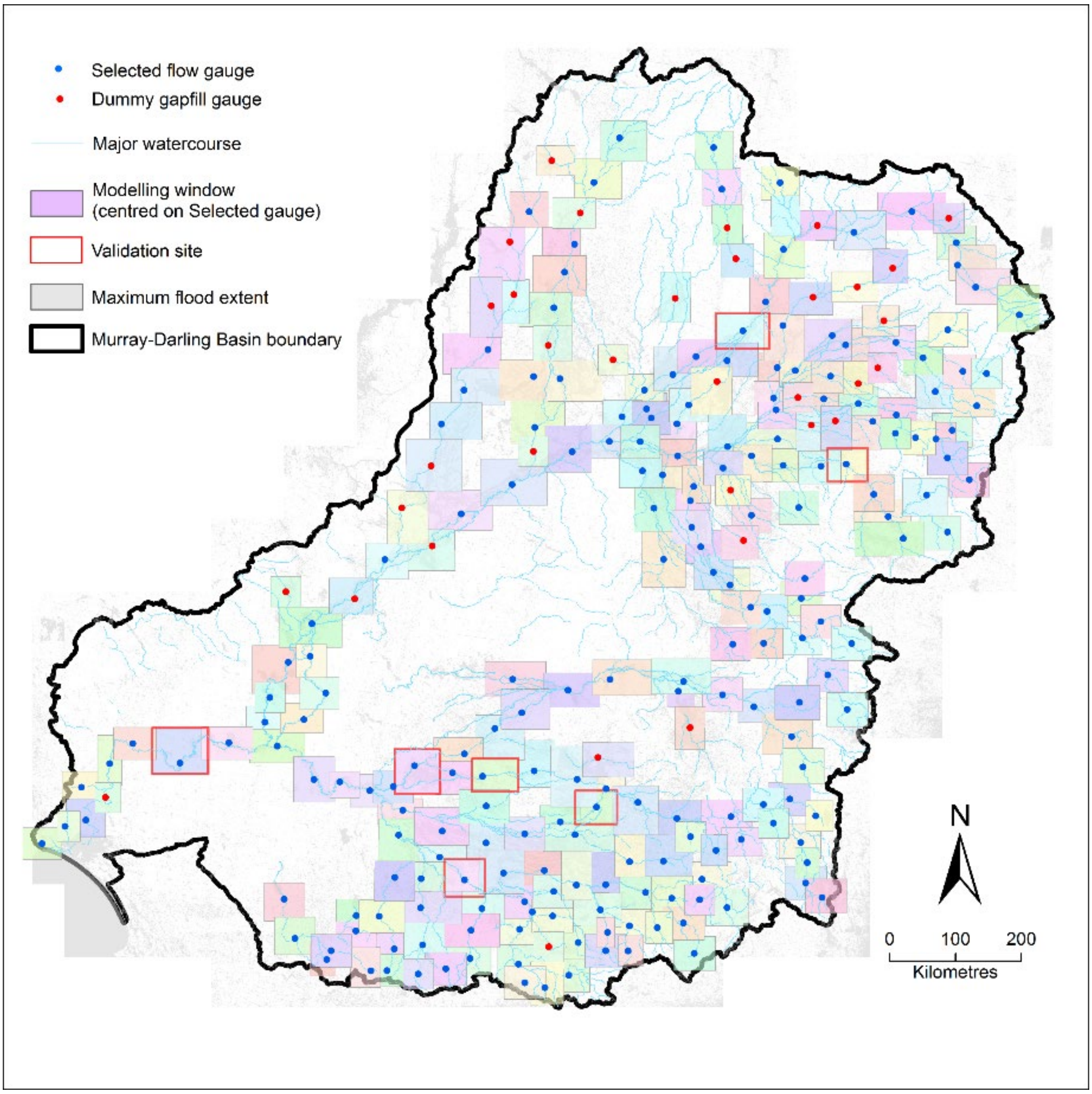

Figure 22 Modelling windows in MDB and initial testing sites.

3.2 Results

The results for comparison of RQ7 results with satellite-derived water extents are shown in Figure 23. Each box represents the interquartile range (IQR) of F-stat values, with the lower and upper bounds showing the 25th and 75th percentiles. Whiskers extend to the minimum and maximum F-stat values, excluding outliers. Outliers, if present (e.g., in LBS_422204), are plotted as individual points. This plot provides an overview of the RQ7 model's performance relative to satellite-derived water extents across different testing reaches. Most reaches demonstrate strong F-stat values (generally above 0.7), indicating a good level of agreement between the RQ7 model predictions and satellite-derived water extents. There are variations in performance, which could be due to region-specific challenges, such as differences in topography, vegetation cover, or data quality.

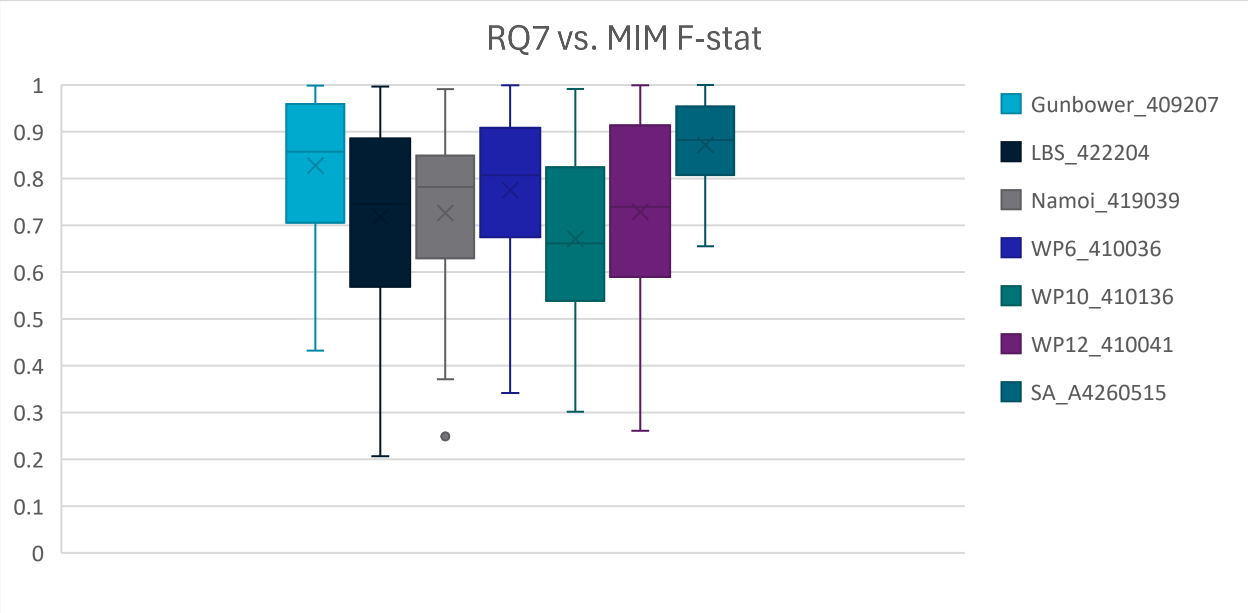

Figure 23 A box-and-whisker diagram comparing the performance of the RQ7 model to satellite imagery derived water extent using F-statistics across seven different reaches.

When compared with the hydrodynamic models (HD) using F-statistics (Figure 24), most medians are relatively low – below 0.4. This suggest that the RQ7 model exhibits moderate to low agreement with hydrodynamic models, with the degree of agreement varying significantly across regions. The lower F-stat values could reflect inherent differences in the modelling approaches: while the RQ7 model uses simplified methods and relies on remote sensing data, hydrodynamic models incorporate detailed physical processes. Discrepancies might also arise from differences in input data, resolution, or assumptions about flood dynamics. We have also looked at under- and over-estimation metrics (not shown) and did not find sign of systematic under- or over-estimation of water extent by RQ7 model compared to the HD models.

The better performance in Gunbower_409207 may reflect more favourable conditions for RQ7's methodology (e.g., better quality remote sensing images and less development in the region, also contributing to good performance relative to satellite-derived water extents), while the poor performance in LBS_422204 could indicate complexities such as human intervention, or infrastructure changes that are not fully captured by the RQ7 model. This variability highlights the need for further refinement of the RQ7 model to improve accuracy, particularly in challenging regions.

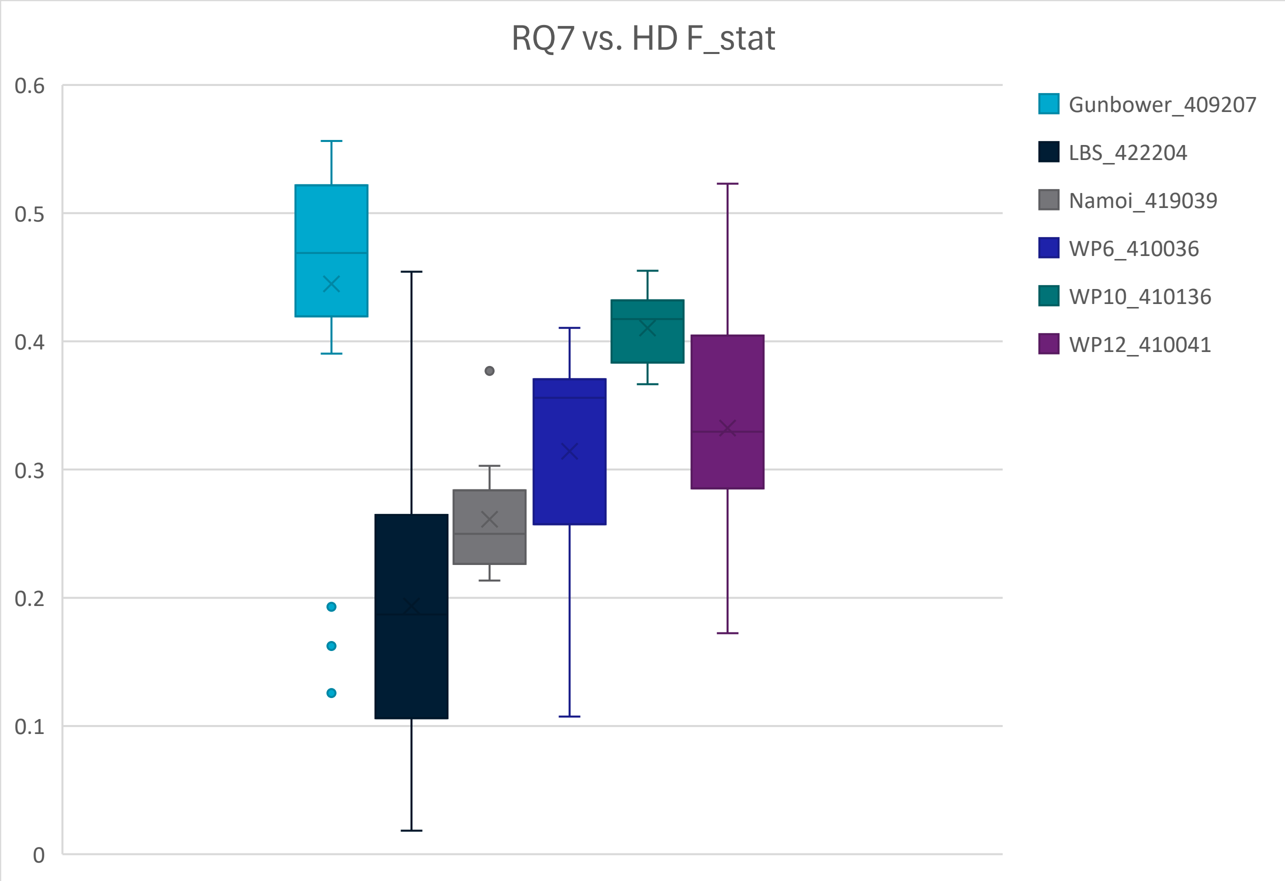

Figure 24 Comparing the water extents modelled by the RQ7 model to those of hydrodynamic models using F-statistics across six different reaches.
Note: the hydrodynamic model calibration event for SA Murray was deemed to be below the over-bank threshold and was not modelled by RQ7 model.

Figure 25 compares the Mean Absolute Error (MAE) of water depth predictions from the RQ7 model against HD models across six different reaches. Gunbower_409207 exhibits the lowest MAE values, with a median around 0.45 m and a narrow interquartile range (IQR). This indicates strong agreement between the RQ7 model and HD models, with relatively low variability and uncertainty in water depth predictions. WP6_410036 has the highest median MAE (~1.5 m), the widest IQR, and several extreme outliers above 3.0. This suggests that water depth predictions in this reach are challenging due to factors such as highly variable hydrodynamics, dense vegetation, or greater reliance on assumptions in both RQ7 and HD models.

While the analysis focuses on the MAE of the RQ7 model relative to HD models, it's important to acknowledge that HD models themselves are not perfect benchmarks. Hydrodynamic models are influenced by uncertainties in their calibration, boundary conditions, and parameterization. Errors in input data, such as DEMs, river cross-sections, or discharge data, can propagate through these models and contribute to discrepancies between HD predictions and observed water depths.

In regions with complex flow dynamics (e.g., WP6_410036 and LBS_422204), the HD model's assumptions and simplifications may not fully capture local hydrological processes, further compounding the apparent discrepancies when compared to the RQ7 model.

Additionally, HD models are often calibrated to specific events or locations, meaning their accuracy may degrade outside of these conditions, introducing additional uncertainty when used as a reference for validation.

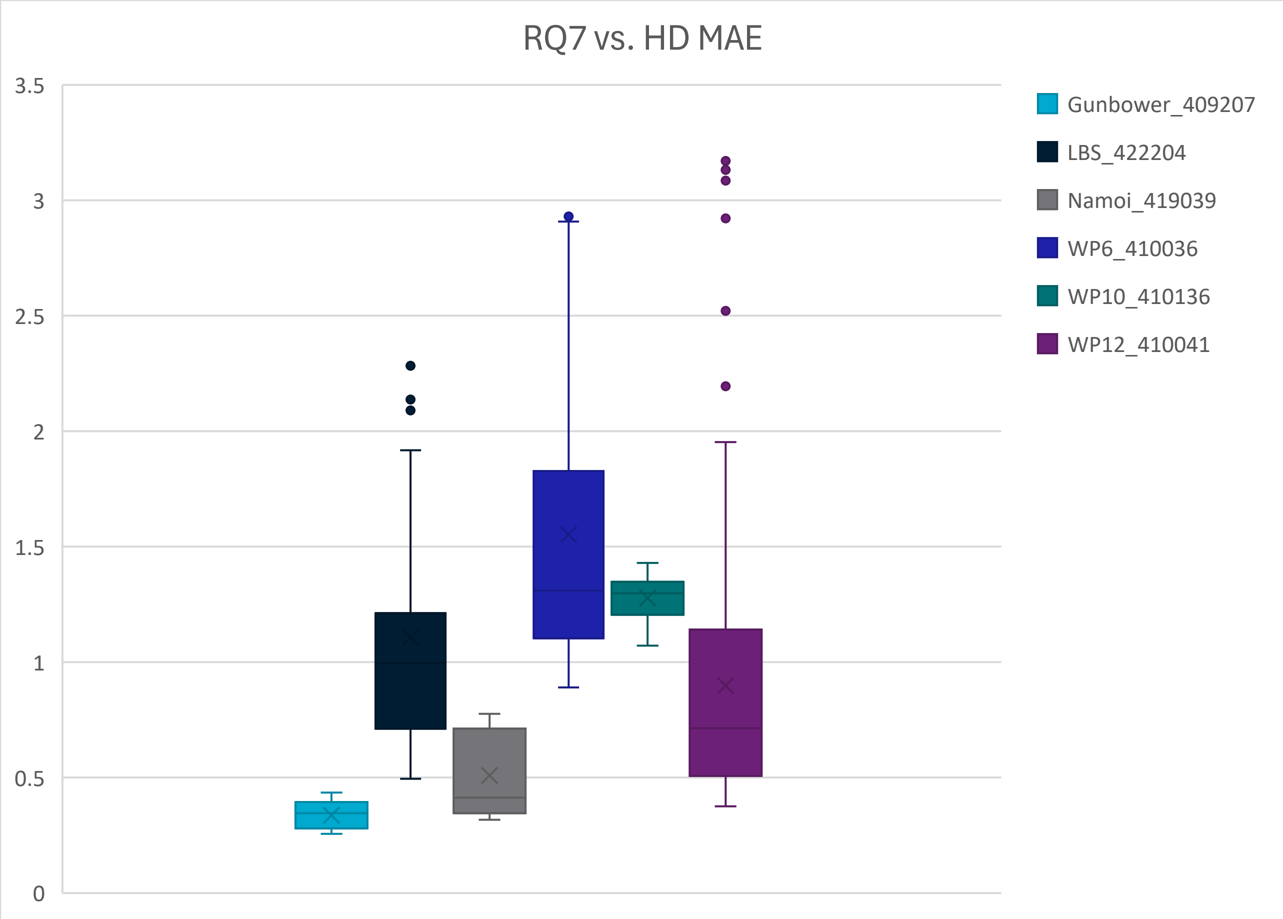

Figure 25 Comparing the water depth modelled by the RQ7 model to those of hydrodynamic models using F-statistics across six different reaches.

F-statistics were calculated using the flood water extent predicted by both the RQ7 model and the hydrodynamic models compared to water extent data derived from remote sensing images or aerial photographs taken during the calibration periods of the hydrodynamic models, and results are shown in Figure 26. There were a total of 42 such images from all six reaches. The RQ7 model consistently achieves higher F-statistics than the HD model across most dates, indicating better agreement with satellite-derived water extents. It is not surprising that the RQ7 model shows stronger alignment with observed satellite-derived water extents, because it is designed to leverage remote sensing data effectively. The HD model's lower agreement may stem from inherent uncertainties or assumptions within hydrodynamic modelling, such as input parameter sensitivity, terrain representation, or boundary condition constraints.

Overall, this comparison highlights the potential of the RQ7 model for supporting floodplain management and decision-making using satellite observations. However, it does not necessarily indicate that the RQ7 model outperforms HD models. This is due to uncertainties associated with satellite-derived water extents and the fact that each modelling approach has its own strengths and limitations depending on the specific context and application.

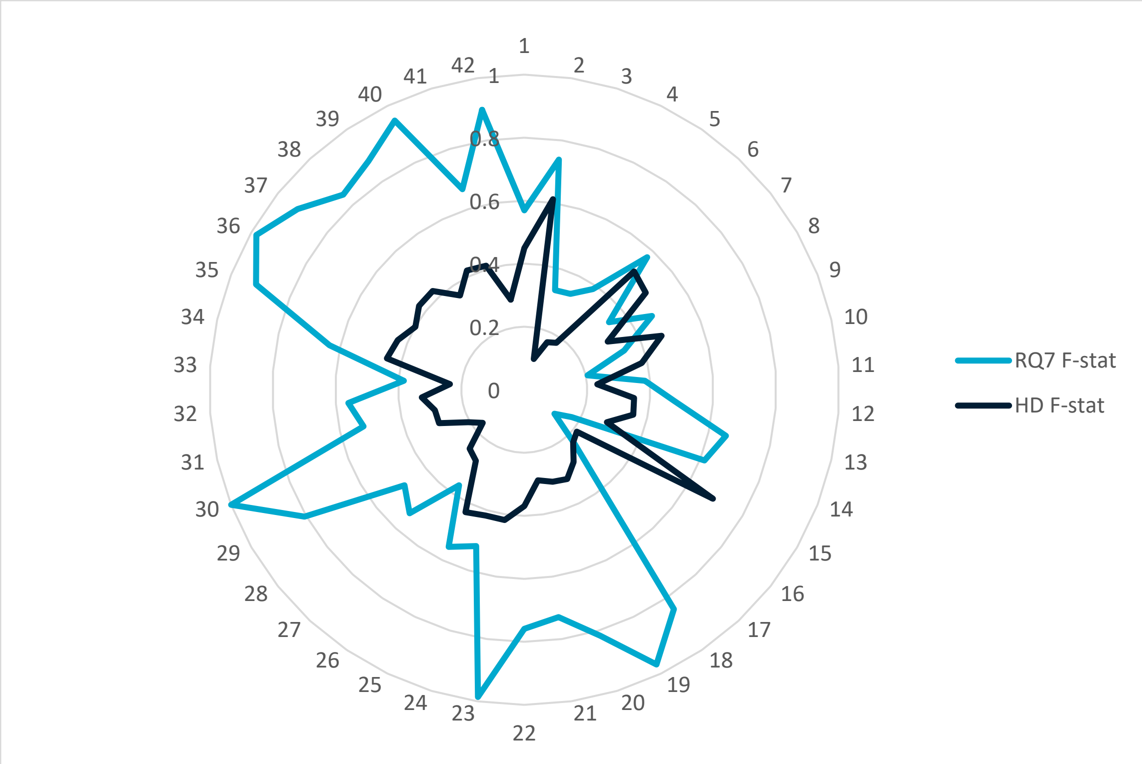

Figure 26 A radar chart compares the F-statistics for the RQ7 model (light blue line) and the hydrodynamic (HD) model (dark blue line) against satellite-derived water extent. Each axis represents a different date on which the F-statistics were calculated.

4 Consideration of volume

The consideration of volume is crucial for effective water resources management. To develop the volume tracking component in the RQ7 model, we first investigated the potential use of existing models (e.g., Source, as employed by the MDBA and Basin States) and data sources (e.g., in situ measurements, remote sensing-derived evapotranspiration (ET), and water extent) to approximate floodplain volume for water accounting purposes. This initial step aimed to evaluate the reliability of these estimates.

The RQ7 model can then be utilized to establish the stage height–inundation area–volume (H-A-V) relationship for major floodplain river reaches. This relationship serves as a direct input to river system models, enabling better accounting for floodplain losses and return flows. The research seeks to minimize uncertainty in floodplain volume predictions by incorporating critical factors such as floodplain soil physical properties, antecedent soil moisture conditions, flood inundation extents, and water depth.

The model estimates the volume of water gained from rainfall, lost to infiltration (recharged into groundwater), and lost to evaporation. These calculations are essential for river system modelling, helping to close the water balance on the floodplain and enabling accurate water accounting. This integrated approach enhances the precision and applicability of floodplain volume estimates for sustainable water resource management.

Local rainfall, evapotranspiration and infiltration all have substantial impacts on the spreading of the flood, and the wetting and drying of the floodplain. We used the module implemented in the TVD model to capture these processes. The soil moisture content for every grid cell was programmed to be continuously updated throughout the model simulation.

An empirical method – the Horton model (Horton, 1941) – was used to relate infiltration rate to elapsed time modified by certain soil properties. The infiltration capacity f_p to time t relationship may be expressed as

$$f_p = f_c + (f_0 - f_c)e^{-\beta t}$$

where f_0 is the maximum infiltration rate at the beginning of an event and reduces to a low and approximately constant rate of f_c as the infiltration process continues, and the soil becomes saturated. The parameter β controls the rate of decrease in the infiltration capacity. Horton's equation is applicable only when effective rainfall intensity is greater than f_c and parameters f_0, f_c and β must be evaluated using observed infiltration data (Maidment, 1993). To satisfy these conditions in the model, the infiltration equation will be set to be effective only when the rainfall intensity is greater than f_c or when the grid cell is covered by flood water. The soil moisture is only affected by evaporation if none of the criteria are met.

As the Horton model typically runs at an hourly time step, while our model operates at a daily time step, we have adapted the equation by using its integral to account for the larger time interval. This approach allows the model to capture the dynamics of infiltration and moisture changes while maintaining consistency with the daily time scale.

5 Limitations and next steps

The RQ7 model is a floodplain inundation prediction model that relies heavily on remote sensing imagery, integrating it with other datasets and methodologies to predict floodplain inundation. While innovative and effective in many respects, the model is subject to several assumptions and limitations tied to the inherent capabilities of remote sensing and the modelling approach itself. These include:

1. Dependence on historical data:
   The RQ7 model can interpolate flood extent and depth within the bounds of historical observations but cannot extrapolate beyond them. For instance, if a hydrograph extends beyond the historical maximum, the model is constrained to predict only the maximum inundation extent and water depth observed in the past. This limitation restricts its applicability under extreme or unprecedented conditions that fall outside the historical record.
2. Impact of remote sensing constraints:
   The accuracy of the RQ7 model is influenced by the limitations of remote sensing imagery:
   - Cloud cover and scan line errors: Satellite images can be obscured by clouds or affected by errors like scan line gaps in Landsat imagery, rendering some data unreliable or unusable.
   - Temporal gaps: The return period of satellites, particularly earlier missions, can lead to gaps in temporal coverage, limiting the availability of images during key flood events.
   - Vegetation cover: Dense vegetation can obscure water detection, reducing the accuracy of surface water mapping in forested or heavily vegetated floodplains. While improvements are ongoing, these challenges remain a significant limitation.
3. Inability to model human interventions:
   The RQ7 model does not account for human activities such as dam operations, water pumping, or irrigation, which can significantly influence floodplain inundation patterns. Currently, areas affected by such interventions are excluded from the model, which limits its scope and applicability in regions with substantial human influence.
4. Infrastructure and terrain changes:
   The model does not dynamically adapt to changes in infrastructure (e.g., levees, channels) or terrain (e.g., sediment deposition or erosion). The solution has been to only use satellite images captured after the last known change, which can result in a limited dataset and reduce predictive power.
5. No consideration of disconnected areas:

   The RQ7 model does not account for areas disconnected from the main river channel, as defined by persistent water observed in long-term remote sensing data.

This may result in inaccurate representation of dead storage during the recession phase of a flood event.

5. Use of arbitrary thresholds:
   A threshold is introduced in the model to distinguish between in-channel and overbank flow, filtering out images below this range. This threshold is based on a historical 2-in-1 year flood occurrence map, which, while practical, introduces a degree of arbitrariness and potential inaccuracies into the modelling process.

To address these limitations, future research and enhancements to the RQ7 model could focus on the following:

- Expanding the remote sensing library: A more extensive library of satellite imagery over time would improve the reliability and accuracy of predictions. Incorporating data from newer satellites with higher spatial and temporal resolution can also mitigate some of the constraints of earlier missions.
- Using deep learning for data correction: Advanced machine learning techniques, such as Generative Adversarial Networks (GANs), could be employed to remove clouds, fill scan line errors, and enhance the continuity and usability of remote sensing data.
- Enhancing water detection in vegetated areas: Continued development of algorithms for detecting water beneath vegetation cover would improve the accuracy of inundation predictions in forested floodplains.
- Integrating hydrological and human-influenced data: Incorporating hydrological models and datasets that account for dam operations, irrigation, and other human interventions could improve the model's ability to simulate real-world conditions.
- Simulating hydrological processes in disconnected areas: Implementing a simplified water balance model to increase or decrease water level based on estimated water balance components such as rainfall, evaporation, and infiltration within these disconnected regions.

By addressing these challenges, the RQ7 model can evolve into a more robust tool, offering higher accuracy and broader applicability for floodplain inundation prediction and management in the MDB and beyond.

Acronyms

AI/ML: Artificial Intelligence/Machine Learning

ANAE: Australian National Aquatic Ecosystem

AWRA: Australian Water Resource Assessment

AWS: Amazon Web Services

BoM: Bureau of Meteorology

DAP: Data Access Portal

DWL: Digital Water and Landscapes

DEM: Digital Elevation Model

DTM: Digital Terrain Model

EASI: Earth Analytics Science and Innovation platform

EC2: Elastic Compute Cloud (EC2)

EO: Earth Observation

FABDEM: Forest And Buildings removed Copernicus DEM

FwDET: Floodwater Depth Estimation Tool

GA: Geoscience Australia

GDEM: Global Digital Elevation Model

GIS: Geographical Information System

HAND: Height Above Nearest Drainage

LiDAR: Light Detection and Ranging

MDB: Murray-Darling Basin

MDBA: Murray-Darling Basin Authority

MDB-EF: MDB Ecosystem Function Project

MD-WERP: Murray-Darling Water and Environment Research Program

MIM: Multi-Index Method

WOfS: Water Observations from Space

RiM-FIM: River Murray Floodplain Inundation Model

RQ7: Research Question 7 – Enhancing Floodplain Inundation and Volume Prediction to Support Environmental Watering and Water Resources Planning

SRTM: Shuttle Radar Topography Mission

SPH: Smoothed Particle Hydrodynamics

TCW: Tasseled Cap Wetness index

TVD: Teng Vaze Dutta

References

Burke, T., Wanigatunga, S., Kolega, A., 2022. SDLAM Reconnecting River Country - Hydraulic Modelling: Work Package 10 – Hay Weir to Maude Weir - Model User Report.

Chiew, F.H.S., McMahon, T.A., 1991. The applicability of morton and penman evapotranspiration estimates in rainfall-runoff modeling. Water Resources Bulletin 27, 611–620.

Chiew, F.H.S., Teng, J., Vaze, J., Post, D.A., Perraud, J.M., Kirono, D.G.C., Viney, N.R., 2009. Estimating climate change impact on runoff across southeast Australia: Method, results, and implications of the modeling method. Water Resour Res 45. https://doi.org/10.1029/2008WR007338

Cohen, S., Brakenridge, G.R., Kettner, A., Bates, B., Nelson, J., McDonald, R., Huang, Y.F., Munasinghe, D., Zhang, J., 2018. Estimating Floodwater Depths from Flood Inundation Maps and Topography. J Am Water Resour Assoc 54, 847–858. https://doi.org/10.1111/1752-1688.12609

Dey, S., Saksena, S., Merwade, V., 2019. Assessing the effect of different bathymetric models on hydraulic simulation of rivers in data sparse regions. J Hydrol (Amst) 575, 838–851. https://doi.org/10.1016/j.jhydrol.2019.05.085

Dunn, B., Lymburner, L., Newey, V., Hicks, A., Carey, H., 2019. Developing a Tool for Wetland Characterization Using Fractional Cover, Tasseled Cap Wetness and Water Observations from Space. International Geoscience and Remote Sensing Symposium (IGARSS) 6095–6097. https://doi.org/10.1109/IGARSS.2019.8897806

Dutta, D., Vaze, J., Karim, F., Teng, J., Kim, S., Mateo, C., Marvanek, S., Ticehurst, C., 2016. Description of Deliverable : Outputs of Inundation Modelling using Synthetic Flood Events for Lower Balonne System.

Fisher, A., Flood, N., Danaher, T., 2016. Comparing Landsat water index methods for automated water classification in eastern Australia. Remote Sens Environ 175, 167–182. https://doi.org/10.1016/j.rse.2015.12.055

Gallant, J., 2019a. Merging lidar with coarser dems for hydrodynamic modelling over large areas. 23rd International Congress on Modelling and Simulation - Supporting Evidence-Based Decision Making: The Role of Modelling and Simulation, MODSIM 2019 1161–1166. https://doi.org/10.36334/modsim.2019.k24.gallant

Gallant, J., 2019b. Merging lidar with coarser dems for hydrodynamic modelling over large areas. 23rd International Congress on Modelling and Simulation - Supporting Evidence-Based Decision Making: The Role of Modelling and Simulation, MODSIM 2019 1161–1166. https://doi.org/10.36334/modsim.2019.k24.gallant

Gallant, J., Wilson, N., Dowling, T., Read, A., Inskeep, C., 2011. SRTM-derived 1 Second Digital Elevation Models Version 1.0 [WWW Document]. Geoscience Australia. URL https://ecat.ga.gov.au/geonetwork/srv/eng/catalog.search#/metadata/72759 (accessed 5.19.22).

Hawker, L., Uhe, P., Paulo, L., Sosa, J., Savage, J., Sampson, C., Neal, J., 2022. A 30 m global map of elevation with forests and buildings removed. Environmental Research Letters 17. https://doi.org/10.1088/1748-9326/ac4d4f

Horton, R.E., 1941. An Approach Toward a Physical Interpretation of Infiltration-Capacity. Soil Science Society of America Journal 5, 399–417. https://doi.org/10.2136/sssaj1941.036159950005000c0075x

Jeffrey, S.J., Carter, J.O., Moodie, K.B., Beswick, A.R., 2001. Using spatial interpolation to construct a comprehensive archive of Australian climate data. Environmental Modelling & Software 16, 309–330.

Lymburner, L., Ticehurst, C., Adame, M.F., Sengupta, A., Kavehei, E., 2024. Seeing the floods through the trees: Using adaptive shortwave infrared thresholds to map inundation under wooded wetlands. Hydrol Process 38. https://doi.org/10.1002/hyp.15174

Maidment, D.R., 1993. Handbook of hydrology. McGraw-Hill New York.

Marvanek, S., Teng, J., Penton, D., Mateo, C., Khanam, F., Ticehurst, C., Vaze, J., 2022. LIDAR enhanced SRTM Digital Elevation Model (DEM) for Murray Darling Basin [WWW Document]. CSIRO. Data Collection.

Montazeri, M., Gibbs, M., 2020. Production of 80 000 ML / day flood inundation map for the South Australian section of River Murray.

Morton, F.I., 1983. Operational estimates of areal evapo-transpiration and their significance to the science and practice of hydrology. J Hydrol (Amst) 66, 1–76.

Nobre, A.D., Cuartas, L.A., Hodnett, M., Rennó, C.D., Rodrigues, G., Silveira, A., Waterloo, M., Saleska, S., 2011. Height Above the Nearest Drainage - a hydrologically relevant new terrain model. J Hydrol (Amst) 404, 13–29. https://doi.org/10.1016/j.jhydrol.2011.03.051

NSW OEH, 2017. Lower Namoi Valley floodplain model development Final report NSW Office of Environment and Heritage Final Report.

Overton, I.C., Mcewan, K., Gabrovsek, C., Sherrah, 2006. Water for a Healthy Country The River Murray Floodplain Inundation Model (RiM-FIM) Hume Dam to Wellington CSIRO Water for a Healthy Country Technical Report.

Penton, D.J., Overton, I.C., 2007. Spatial Modelling of Floodplain Inundation Combining Satellite Imagery and Elevation Models.

Potter, N.J., Zhang, L., 2009. Interannual variability of catchment water balance in Australia. J Hydrol (Amst) 369, 120–129. https://doi.org/10.1016/j.jhydrol.2009.02.005

Sims, N., Anstee, J., Barron, O., Botha, E., Lehmann, E., Li, L., Mcvicar, T., Paget, M., Ticehurst, C., Van Niel, T., Warren, G., 2018. Earth observation remote sensing A technical report to the Australian Government from the CSIRO Northern Australia Water Resource Assessment, part of the National Water Infrastructure Development Fund: Water Resource Assessments.

Sims, N.C., Warren, G., Overton, I.C., Austin, J., Gallant, J., King, D.J., Merrin, L.E., Donohue, R., McVicar, T.R., Hodgen, M.J., D.J., P., Chen, Y., Huang, C., Cuddy, S., 2014. RiM-FIM Floodplain Inundation Modelling for the Edward-Wakool, Lower Murrumbidgee and Lower Darling River Systems. Report prepared for the Murray-Darling Basin Authority.

Teng, J., Chiew, F.H.S., Yang, A., Zheng, H., Penton, D.J., Ticehurst, C., Marvanek, S., Vaze, J., Khanam, F., Post, D.A., Pollino, C., 2024. Floodplain inundation in the Murray-Darling Basin under current and future climates .

Teng, J., Jakeman, A.J., Vaze, J., Croke, B.F.W., Dutta, D., Kim, S., 2017. Flood inundation modelling: A review of methods, recent advances and uncertainty analysis. Environmental Modelling and Software 90. https://doi.org/10.1016/j.envsoft.2017.01.006

Teng, J., Vaze, J., Dutta, D., Marvanek, S., 2015a. Rapid Inundation Modelling in Large Floodplains Using LiDAR DEM. Water Resources Management 29. https://doi.org/10.1007/s11269-015-0960-8

Teng, J., Vaze, J., Dutta, D., Marvanek, S., 2015b. Rapid Inundation Modelling in Large Floodplains Using LiDAR DEM. Water Resources Management 29. https://doi.org/10.1007/s11269-015-0960-8

Teng, J., Vaze, J., Kim, S., Dutta, D., Jakeman, A.J., Croke, B.F.W., 2019. Enhancing the Capability of a Simple, Computationally Efficient, Conceptual Flood Inundation Model in

Hydrologically Complex Terrain. Water Resources Management 33. https://doi.org/10.1007/s11269-018-2146-7

Teng, J., Vaze, J., Kim, S., Dutta, D., Jakeman, A.J., Croke, B.F.W., 2018. Enhancing the capability of a simple, computationally efficient, conceptual flood Inundation model in hydrologically complex terrain. Water Resources Management. https://doi.org/http://dx.doi.org/10.1007/s11269-018-2146-7

Teng, J., Yang, A., Penton, D., Ticehurst, C., Marvanek, S., Vaze, J., Chiew, F., Bridgart, R., Mateo, C., Khanam, F., Brennan, E., Post, D., 2025. A novel approach leveraging remote sensing data to enhance flood inundation prediction. Environmental Modelling & Software. In preparation.

Tetley, D., 2022. Sustainable Diversion Limits Adjustment Mechanism (SDLAM) - Hydraulic Modelling: Model User Report.

Ticehurst, C., Teng, J., Sengupta, A., 2022. Development of a Multi-Index Method Based on Landsat Reflectance Data to Map Open Water in a Complex Environment. Remote Sens (Basel) 14. https://doi.org/10.3390/rs14051158

Vaze, J., Mateo, C.M., Wang, B., Teng, J., Marvanek, S., 2018. AWRA-L input spatial layers at 1 km and 5 km resolutions for the Australian continent - Source data and comparison between 1 km and 5 km resolutions 121.

Wells, M., Streeton, N., 2022. SDLAM Reconnecting River Country - Hydraulic Modelling: Work Package 12 – Lowbidgee Wetlands - Model User Report.

Xu, H., 2006. Modification of normalised difference water index (NDWI) to enhance open water features in remotely sensed imagery. Int J Remote Sens 27, 3025–3033. https://doi.org/10.1080/01431160600589179

Yamazaki, D., Ikeshima, D., Sosa, J., Bates, P.D., Allen, G.H., Pavelsky, T.M., 2019. MERIT Hydro: A High-Resolution Global Hydrography Map Based on Latest Topography Dataset. Water Resour Res 55, 5053–5073. https://doi.org/10.1029/2019WR024873

Zheng, H., Chiew, F., Post, D., Robertson, D., Charles, S., Grose, M., Potter, N., 2024. Projections of future streamflow for Australia informed by CMIP6 and previous generations of global climate models. J Hydrol (Amst) 636, 131286. https://doi.org/https://doi.org/10.1016/j.jhydrol.2024.131286

As Australia’s national science agency and innovation catalyst, CSIRO is solving the greatest challenges through innovative science and technology.

CSIRO. Unlocking a better future for everyone.

Contact us

1300 363 400
+61 3 9545 2176
csiroenquiries@csiro.au
www.csiro.au

For further information

Environment
Dr David Post
David.Post@csiro.au
www.csiro.au/en/research/natural-environment/water/Murray-Darling-Basin/MD-WERP